Chapter 5

Study of virulence factors

Chapter 5

5.1 Introduction

Kp is the most common causative agent of nosocomial Gram-negative urinary tract infections (UTIs) after E. coli (Niveditha et al., 2012; Podschun and Ullmann, 1998). Capsular polysaccharides (CPS), exopolysaccharides (EPS) and biofilm are the major virulence factors in pathogenesis of *Klebsiella* (Clegg et al., 2016). The layer of polysaccharides forms capsule that lies outside the cell envelope are called capsular polysaccharides (CPS). It is a part of outer envelope of bacterial cell, not easily washed-off and plays important role in inhibition of phagocytosis by host immune system (Ares et al., 2019). Exopolysaccharides is defined as polymers linked to the cell surface via covalent bond to phospholipid or lipid A molecules. Exopolysaccharides appears to be released on the cell-surface with no attachment to the cell and they are often sloughed off in form of slime (Taylor and Roberts, 2005). *rmpA* (regulator of mucoid phenotype), a gene known as extracapsular polysaccharide synthesis regulator, positively controls the mucoid phenotype of *K. pneumoniae*. (Yu et al., 2006). Expression of *cps* genes is positively regulated by *rmpA* gene. DNA binding domain in the C-terminal region of *rmpA* activates transcription of *cps* genes by binding to the promoter region of cps gene cluster (Cheng et al., 2010). *Wzi* is a gene conserved in all capsular types of *Klebsiella pneumoniae (Kp)* that codes for an outer membrane protein involved in capsule attachment to the cell surface, and used for simple and rapid method for the prediction of K-type (Brisse et al., 2013). *wzi* alleles such as *wzi154*, *wzi29* and *wzi50* could be used as potential targets for vaccines against CRKP (Banerjee et al., 2021). String test is a characteristic to detect hypervirulent strain of *Klebsiella*. A positive string test is defined as the formation of viscous strings of >5mm in length when a loop is used to stretch the colony on an agar plate. (Fang et al., 2004). String positive strains are often associated with complicated infections in case of pyogenic liver abscess (PLA) (Hsu et al., 2011) Overproduction of capsule leads to formation of thick capsule, which is reported to be responsible for virulence by resistance of phagocytosis (Paczosa and Mecsas, 2016). Polymorphonuclear leukocytes (PMNs) are a type of white

blood cell (WBC) and neutrophils are a type of PMNs. Resistance of phagocytosis by neutrophils is a major virulence mechanism observed in *Klebsiella* pathogenesis (Clegg et al., 2016).

Biofilms are a major issue in UTIs and are reported to be involved in 65% of bacterial infections, allowing cells to persist and leading to increased antibiotic resistance (Høiby et al., 2011). Further, catheter-associated urinary tract infections (CAUTIs) by *Kp* represent one of the most common hospital-acquired infections (HAIs) leading to increased patient morbidity (Nicolle, 2014). Bacterial biofilm formation on the interior and exterior surfaces of the catheter has been identified as the most important cause of CAUTIs (Ong et al., 2008). Biofilm is an aggregate of microorganisms attached to an inert or living surface by a self-produced exo-polymeric matrix, which include polysaccharides, proteins, and extracellular DNA (eDNA) (Bandeira et al.,2014). Biofilms inhibit effective antibiotic penetration, reduce the bacterial growth rate, lead to the development of persister cells, and facilitate genetic exchange (Lewis.,2008; Calà et al., 2015). Hence, a detailed understanding of the biofilm may help in developing strategies to combat biofilm formation. Recently, several studies report the association of antibiotic resistance with biofilm formation in clinical isolates of *Klebsiella* spp. (Karimi et al., 2021; Vuotto et al., 2017; Ostria-Harnandez et al., 2018; De Campos et al., 2016; Khodadadian et al., 2018). Moreover, the role of fimbriae in adhesion and biofilm formation by *Klebsiella* is also well documented (Schroll et al., 2010; Stahlhut et al., 2012). However, studies on characterization and quantification of *Kp* biofilms are lacking.

The present work is undertaken to explore the influence of factors like CPS, EPS, string and *rmpA* in virulence by inhibiting phagocytosis. The study of biofilms focused on the differences between strong and weak biofilms formed by clinical isolates of *Kp* on various catheters and in different media conditions and differences in their matrix components.

5.2 Materials and methods

5.2.1 Extraction of CPS

Extraction of CPS was done as described in Brimacombe and Beatty, 2013. Bacterial cultures were grown to early stationary phase in suitable growth medium and OD650 of culture was measured. Cultures were normalized to same initial OD650. 10 ml of culture broth was centrifuged at 10,000 g for 10 minutes and supernatant was discarded carefully. Pellet of cells was washed in 1 ml of 50 mM NaCl by centrifugation at 10,000 g for 10 minutes and supernatant was removed. This step was repeated, and total five washes were given to the cells. Pellet was resuspended in 1 ml of 50 mM EDTA, and incubated at 37 °C for 60 minutes. Pellet was further centrifuged at 10,000 g for 10 minutes, and supernatant was transferred to a fresh microfuge tube. Supernatant contained capsular polysaccharide (CPS).

5.2.2 Extraction of EPS

Bacteria was grown to desired growth phase (early stationary phase) in suitable growth medium. Initial OD650 of cultures used for extraction of EPS was same as used for extraction of CPS to produce comparable results 10 ml of culture broth was centrifuged at 8000 rpm for 15 minutes for obtaining cell-free broth. Supernatant was transferred to another tube, and to the supernatant, 3 volumes of ice-cold isopropanol was added and kept at 4 °C overnight for precipitation of EPS. Next day, the mixture was centrifuged at 10,000 rpm for 10 minutes. Supernatant was discarded and pellet air dried. Pellet was resuspended in 1 ml of distilled water. This extract contained exopolysaccharide.

5.2.3 Quantification of CPS and EPS

Carbohydrate stock solution was prepared by diluting glucose stock solution into 1 ml aliquots of 0 µg/ml – 40 µg/ml from 1mg/ml stock solution. 200 µl of stock solutions of different concentration of glucose was pipetted out for preparing a standard. Similarly, 200 µl of extracted sample (CPS and EPS individually) and 200 µl of 50mM EDTA (blank) was added into separate tubes. 200 µl of 5% phenol was added in all tubes and mixed well by shaking. 1ml of

93% sulphuric acid was added and mixed by swirling. Color was allowed to develop for 10 min at room temperature. Additional gentle mixing by swirling was done every 2-3 minutes. Absorbance was measured at OD490 in a spectrophotometer. Concentration of carbohydrates was then calculated using a standard curve. (Brimacombe and Beatty, 2013).

5.2.4 Statistical Analysis

All assays/experiments were performed in triplicates and standard deviation (SD) values were calculated. To analyse the correlation between CPS and EPS, Pearson's Correlation test was done. The distribution of CPS and EPS was analysed using frequency distribution in Prism 8.0 Software (GraphPad, San Diego, USA).

5.2.5 Detection of string phenotype

String test was performed for detection of string phenotype and to study if there is any association between amount of CPS and string formation as well as resistance to phagocytosis. Isolates were freshly subcultured to recover their phenotype. Freshly subcultured isolates were then streaked onto sheep blood agar plates (HiMedia Laboratories Pvt. Ltd., Mumbai, India) and incubated at 37 ºC overnight. Next day, to determine the hypermucoviscous phenotype, a sterile bacteriologic loop was used to stretch a mucoviscous string from the colony of freshly subcultured blood agar plate. Formation of viscous strings of >5mm in length was considered as a positive string test (Yu, W. L et al., 2006).

5.2.6 Study of *rmpA*

5.2.6.1 Detection of rmpA using polymerase chain reaction (PCR)

Presence of *rmpA* in the isolates was detected using PCR. Previously isolated gDNA was used as templet for PCR. Primers used for PCR were from Yu et al (Yu et al., 2006). The amplicons were then sent for Sanger's sequencing at to Eurofins Scientific (Chennai, India) to confirm to identity of the amplified gene. The details of primers are as follows:

rmpA F- 5' ACTGGGCTACCTCTGCTTCA 3'

rmpA R- 5' CTTGCATGAGCCATCTTTCA 3'

Reaction mixture used for PCR is shown in table 5.1 and table 5.2

Table 5.1 Reaction mixture used for PCR of *rmpA*

Reagents	Volume (µl)
SapphireAmp® Fast PCR Master Mix (TaKaRa Bio Inc., Tokyo, Japan)	12.5 µl
Forward primer	2 µl (20pmol/ µl)
Reverse primer	2 µl (20pmol/ µl)
Templet DNA	2 µl (70-80 ng/ µl)
AMQ (autoclaved molecular-grade water)	4.5 µl
Total system	25 µl

Table 5.2 PCR conditions used for detection of presence of *rmpA*

Step	Temperature (ºC)	Time
Initial denaturation	94	4 minutes
Denaturation	94	30 seconds
Annealing	50	40 seconds
Primer extension	72	1 minute
GOTO Step 2, Repeat cycle 30 times		
Final extension	72	10 minutes

5.2.6.2 Study of rmpA expression by qRT-PCR

To study expression of *rmpA*, RNA was isolated from *rmpA* positive isolates, cDNA was synthesized from isolated RNA and then finally, qRT-PCR was performed to measure expression of *rmpA* using the cDNA as templet.

(a) RNA isolation

For RNA isolation, first, all glassware and plasticware used in RNA isolation were given treatment with 0.05% Diethyl pyro carbonate (DEPC) treated

molecular grade water and left overnight to get rid of RNase. Next day, to inactivate DEPC, all the treated consumables were autoclaved. 2.5ml of overnight grown culture with $OD_{600} = 0.5$ was centrifuged at 10,000 rpm for 10 minutes. Pellet was resuspended in 1 ml RNAiso Plus TRI reagent (TRISOL) (Takara Bio Inc., Shiga, Japan) and incubated for 10-15 minutes on ice. 1.5µl RNase inhibitor is added after the incubation on ice. 400 µl of chloroform was then added and mixed gently by inverting the tube for 15 seconds and on ice for 2-3 minutes. Tubes were centrifuged at 10,000g for 10 minutes at 4 ºC. the mixture was separated into 3 phases: an aqueous phase containing the RNA, the interphase containing DNA, and an organic phase containing proteins. Upper aqueous phase was carefully transferred to new microfuge tube and 500 µl of chilled isopropanol was added and mixed and incubated on ice for 15-20 minutes. Tubes were then centrifuged at 10,000g for 10 minutes at 4 ºC. Supernatant was removed by pipetting and pellet was washed with 75% ethanol followed by centrifugation at 7500g for 5 minutes at 4 ºC. Supernatant was removed, and pellet of RNA was air dried. Pellet was dissolved in 20µl molecular grade RNase free water.

DNase treatment

DNase treatment was given as shown in Table 5.3 at 37 ºC for 20 minutes. 2 µl of 200mM EDTA was added to stop the reaction and incubated for 10 minutes at 75 ºC.

Table 5.3 Reagents used for DNase treatment

Reagents	Volume (µl)
RNA	(10 µg)
10X buffer	2.5
DNase I	3 (1U/µl)
AMQ water	X µl
Total system	25 µl

After DNase treatment, precipitation was done by adding 500 µl isopropanol for 2 hours at -20 ºC followed by centrifugation at 10,000 rpm for 10 minutes. Supernatant was removed, and 75% ethanol was added to the pellet followed by centrifugation at 7500 rpm for 5 minutes. Obtained pellet of DNA-free RNA was air dried and dissolved in 25 µl RNase-free molecular grade water.

(b) cDNA synthesis

cDNA synthesis from total 2.5 µg RNA was done using PrimeScript™ cDNA Synthesis Kit (Takara Bio Inc., Shiga, Japan) by following the manufacturer's protocol. Table 5.4 shows the reaction system-I used. The reaction system-I was incubated at 65 ºC for 5 minutes and then immediately placed on ice. It was then used to prepare reaction system II as described in table 5.5. The reaction system-II was then incubated for 10 minutes at 30 ºC, followed by 1 hour at 50 ºC, and finally for 5 minutes at 70 ºC. The mixture was then cooled on ice and stored at -20 ºC.

Table 5.4 Reaction system I for cDNA synthesis

Reaction component	Volume/ amount
Random-6-mers	2 µl
dNTP mix	1 µl
Template RNA	2.5 µg
RNase free water	X µl
Total system	10 µl

Table 5.5 Reaction system II for cDNA synthesis

Reaction component	Volume
Reaction system I	10 µl
5X Prime Script Buffer	4 µl
RNase inhibitor	0.5 µl
Reverse-Transcriptase	1 µl
RNase free water	4.5 µl
Total system	20 µl

(c) qRT-PCR

cDNA from *rmpA* positive isolates was used as templet for relative qRT-PCR to determine the expression levels of *rmpA* in the isolates. SYBR Green master mix (Takara Bio Inc., Shiga, Japan) was used for qRT-PCR. *rpoB* (housekeeping gene) was used as the internal control for study of relative gene expression. Isolated RNA of respective isolates was used as templet for negative control to confirm the absence of gDNA. Ct (cycle threshold) values of each sample was recorded and fold-change of *rmpA* expression was calculated using comparative Ct method (Schmittgen and Livak, 2008). MTCC *Klebsiella pneumoniae* strain 39 was used as reference strain for calculating fold change. The relative fold change of *rmpA* for each sample was normalized against a housekeeping gene, *rpoB*. Table 5.6 shows name and sequences of primers used. Name and sequences of the primers were as per Hsu et al (Hsu et al., 2011). Table 5.7 shows the reaction system used for qRT-PCR and table 5.8 shows the PCR conditions.

Table 5.6 Primers used for qRT-PCR of *rmpA*

Primers	Sequences
(*rmpA*)Both F	5'GGTGTGATTATGACATCTATGTT 3'
(*rmpA*) 459R- 5'	5' CATAGATGTCATAATCACACC 3'
rpoB-F	5'AAGGCGAATCCAGCTTGTTCAGC 3'
rpoB-R	5'TGACGTTGCATGTTCGCACCCATCA 3'

Table 5.7 Reaction system used for qRT-PCR

Reaction Component	Volume
SYBR Green master mix	10 μl
AMQ water	4 μl
Forward Primer	2 μl
Reverse Primer	2 μl
cDNA Template	2 μl
Total System	20 μl

Table 5.8 Conditions used for qRT-PCR

Step	Temperature ºC	Time
Initial denaturation	95	3 minutes
Denaturation	94	30 seconds
Annealing	59	30 seconds
Primer extension	72	30 seconds
Repeat cycle 35X		
Final extension	72	5 minutes
Melt curve	65 to 95 increments 0.5	0:05 seconds

5.2.7 Phagocytosis assay

Phagocytosis assay was performed to determine the role of EPS, CPS, *rmpA* and string positivity in resistance of phagocytosis, which is one of the major virulence mechanism of *Klebsiella*. To study phagocytosis by selected isolates, first isolates were labelled with Fluorescein isothiocyanate (FITC), neutrophils were isolated from healthy human donors (n=5). FITC labelled bacteria were allowed to be phagocytosed by isolated neutrophils. The amount of phagocytosis was analysed using flow-cytometry. To visualize phagocytosis event, fluorescence microscopy and confocal laser scanning microscopy (CLSM) were also performed from the same preparation. CLSM was performed for better visualization and to confirm the location of FITC-labelled bacteria.

5.2.7.1 Determination of K-type

Amplification and Sanger's sequencing of *wzi* gene was performed to determine K-type of the isolates. The primers and PCR conditions used for *wzi* amplification were as described by Brisse et al., 2013.

*wzi*_Forward: 5'-GTGCCG CGA GCG CTT TCT ATC TTG GTA TTC C-3'
*wzi*_Reverse; 5'- GAGAGC CAC TGG TTC CAG AA[C or T] TT[C or G] ACC GC-3'

Amplification using PCR was done at 94°C for 2 min (initial denaturation); 30 cycles were performed [each 94°C for 30 seconds (denaturation), 55°Cfor 40

seconds (annealing), and 72°C for 30 seconds (primer extension)], followed by a final elongation step (72°C for 5 min). 2 µl of isolates DNA of respective isolates was used at templet. The K-type was then determined by uploading the sequence of the amplicon (*wzi* gene) on scheme available on BIGSdb database: https://bigsdb.pasteur.fr/klebsiella/klebsiella.html (Jolleyand Maiden, 2010).

5.2.7.2 FITC labelling

Respective bacterial cultures were labelled with FITC according to previously reported method (Lin et al., 2004); cultures were also processed as unlabelled to use as control. Bacterial culture was incubated overnight at 37 ºC. The concentration was measured using photo spectrometry (Bio-Rad, Hercules, USA). The percentage of bacterial viability in an aliquot of each culture was determined by quantitative plate counting. The bacterial culture was then heat-killed by heating at 75 ºC for 1 hour in water bath and quantitative colony count determination of culture viability was performed again. Then, culture was distributed to two fresh sterile falcon tubes (FITC-labelled and unlabelled) and centrifuged at 10000 rpm for 10 minutes. Supernatant was discarded, and wash of phosphate buffer saline (PBS) (HiMedia Laboratories Pvt. Ltd., Mumbai, India) was given to the cell pellet by centrifugation to remove residues of media. FITC of final concentration 0.1 mg/ml in 0.10 M $NaHCO_3$ (pH 9.0) was added to each tube (labelled) to make up the final volume of 2 ml. To the unlabelled tube, 2 ml of only 0.10 M $NaHCO_3$ (pH 9.0) was added. Both tubes were incubated in dark for an hour at room temperature. Culture was then transferred in fresh sterile microfuge tubes and the unbound FITC was washed off by three washes of PBS by centrifugation at 10,000 rpm for 10 minutes. All the steps were carried out in dark and tubes were covered with aluminium foil to avoid photobleaching of FITC. Labelled and unlabelled bacterial cultures were re-suspended in 200 µl of PBS and stored at -80 ºC. The FITC-labelled bacteria were resuspended to a concentration of 2×10^8 cells/ml in PBS and divided into equal volumes. Aliquots were thawed just before the use.

5.2.7.3 Isolation of human neutrophils

The isolation of neutrophils was done from five healthy human volunteers. Neutrophils were isolated as described by Lin et al (Lin et al., 2004). 60 ml of

freshly drawn, heparinized blood was mixed with an equal volume of a dextran–saline solution. Sedimentation of particulates was allowed by keeping it at room temperature for 40 min. The white blood cells (WBCs)-rich supernatant was layered on ficoll-hypaque (Sigma-Aldrich, St. Louis, USA) and centrifuged at 400g, for 25 min, at 4 °C in density gradient centrifuge. From the density construct, the upper mononuclear layer was removed and discarded, leaving PMNs (mainly neutrophils) and erythrocytes in the pellet. RBC lysis buffer was added to remove erythrocytes. After that, neutrophils were resuspended using ice-cold PBS. Further, neutrophils were washed 3 times with PBS by pelleting down at 250g for 15 min at 4 ºC. Neutrophils were then dissolved in PBS to a concentration of 1 X 10^7 cells/ml. Visualization and counting of WBCs were performed using Neubauer's chamber after the isolation of neutrophils.

5.2.7.4 Phagocytosis assay

Phagocytosis assay was performed according to Lin et al (Lin et al., 2004). 100 µl of neutrophils suspension containing 10^6 cells, 100 µl serum (above isolated) and 200 µl FITC labelled bacteria (4x10^7 cfu/ml) were added in microfuge tubes covered in aluminium foil. 600 µl of PBS was added in the flow cytometry tube (Becton Dickinson, New Jersey, United States) to make a final volume of 1ml. The tubes were incubated in shaking water bath for 15, 30 and 60 minutes. One unincubated tube was kept for 0-minute control. At each time point samples were removed and centrifuged at 250g for 6 minutes and cell pellet was resuspended in 1 ml of PBS. All samples were then strained individually to flow cytometry tubes using strainer (HiMedia Laboratories Pvt Ltd, Mumbai, India) and processed further for flow-cytometric (FACS) analysis and microscopic analysis, respectively.

(a) Flow-cytometric analysis of phagocytosis

A FACScan emitting an argon laser beam at 488 nm (Becton Dickinson FACSCalibur, New Jersey, United States) was used to detect the FITC fluorescence. The sideways scatter (SSC) threshold was 52. The detector was set at E00, 350, and 427 for forward scatter (FSC), SSC, and fluorescence 1 (FL1-H, green), respectively. Fluorescence values were recorded after gating the detector on the FSC and SSC combination. Unstained and FITC-stained

bacteria phagocytosis mixtures were processed to determine the cut-off of positive and negative fluorescence. Fluorescence distribution data collected were displayed as single histograms for FL1-H. A total of 10000 cells were processed for each sample. The population was gated to include only population of granulocytes. All the samples were ran using the same settings to make the data comparable. Three independent experiments were performed to evaluate the % phagocytosis of the isolates.

(b) Visualization of phagocytosis using fluorescence microscopy and CLSM

Microscopic evaluation of phagocytosis was performed as described in Lin et al (Lin et al., 2004). Same protocol and preparations was used for microscopic analysis as described above. Slides were prepared from 200 µl of FITC-labelled bacteria (4×10^7 cfu/ml) of selected isolates added to a clean slide containing 10^6 neutrophils individually. The tubes were incubated for 15 minutes. Ethidium bromide (EtBr) was added to final concentration 50 µg/ml just before the microscopic analysis. The slides were then observed under fluorescence microscopy and CLSM. Excess EtBr was used to suppress the extracellular fluorescence. Bacteria that were not localized in neutrophils stained with EtBr (extracellular dye) and appeared red in color upon microscopic examination and bacteria phagocytosed by neutrophylls appeared in green color because of FITC labelling.

Study of Biofilm

5.2.8 Quantification of biofilm formation

Crystal violet assay was performed to quantify biofilm formation by all 28 clinical isolates of *Kp* and further categorized into strong, moderate, or weak

biofilm producers using statistical analysis described by Stepanović et al (Stepanović et al., 2004). Briefly, 25 µl of overnight grown culture (O.D. at 600 nm ~ 0.3) was added to 225 µl of sterile LB in a sterile 96-well flat bottom microtiter plate (Laxbro Bio-Medical Aids pvt. Ltd., Pune, India) and incubated at 37 ∘C for 24 h. The assay was performed in triplicates.

Only LB without bacterial culture was used as negative control for biofilm formation and MTCC *K. pneumoniae* 39 strain was taken as a standard strain from Microbial Type Culture Collection (MTCC). After 24 h, the adhered biofilm was fixed by adding 250 µl of methanol for 15 min. The biofilm formed was then stained by 250 µl of 0.5% crystal violet solution for 15 min. The excess stain was washed away by flushing the wells with 0.8% saline twice and then allowed to be air dried. The stain attached to adherent layers was re-solubilized in 250 µl of 33% acetic acid for 15 min. The optical density (OD) of the solution was measured at 570 nm using a microtiter plate reader (Multiskan Go, Thermo Fisher Scientific, Waltham, USA). The isolates were categorized into weak, moderate, or strong biofilm producers based on the cut-offOD (ODc) is defined as three standard deviations above mean OD of negative control (at 570 nm). Isolates were classified as follows: OD ≤ ODc = no biofilm producer, O.Dc < O.D. ≤ (2 × ODc) = weak biofilm producer, 2ODc < OD ≤ (4 × ODc) = moderate biofilm producer, (4 × ODc) < OD = strong biofilm producer (Stepanović et al., 2004). Moreover, the biofilm index was calculated for all 28 isolates using this formula. Biofilm index = OD_{570}(CV assay)/OD 600(culture) (Crémet et al., 2013).

5.2.9 Growth curve

Growth curve assay was performed for all six isolates using synergy HTmicroplate reader (BioTek instruments, Winooski, USA). 250 µl of overnight grown culture (OD at 600 nm ~ 0.3) was added to 1 mL of fresh LB and incubated at 37 ◦C until the OD at 600 nm reaches 0.05. 100 µL of all six isolates (OD at 600 nm ~ 0.05) was inoculated in a sterile 96-well flat bottom microtiter plate and incubated at 37 ◦C for 24 h in continuous shaking conditions in an automated microplate reader. OD at 600 nm was measured constantly at an interval of 15 min for 12 h until the cultures reach to the stationary phase and growth curve was plotted. The growth rate and generation time for each isolate was calculated from the graph.

5.2.10 Quantification of biofilm on catheters

Biofilm formed on three types of catheters (latex, silicone-coated latex, and silicone) was quantified by a modified crystal violet assay. 13 mm long piece of each type of catheter was cut vertically and fixed at the base of a 24-well plate (Laxbro Bio-Medical Aids Pvt. Ltd., Pune, India). 1 mL of 1:10 diluted culture (OD at 600 nm ~ 0.3) was inoculated in wells containing catheter piece and incubated at 37 ∘C for 24 h. After 24 h, unbound cells were washed with water. The piece of catheter was then transferred to a fresh 24-well plate to avoid the evaluation of the biofilm formed at the bottom of the previous plate. Bound biofilm was fixed with 1 mL methanol and then stained with 1 mL 0.5% crystal violet. The excess stain was washed with 0.8% saline, the bound stain was re-solubilized in 1 mL 33% acetic acid and its OD was measured at 570 nm. Biofilm formed in the presence of sterile LB, sterile artificial urine (2.43% urea, 1% NaCl, 0.6% KCl, 0.64% Na_2HPO_4, 0.05 mg/mL albumin, pH 5–7) (Shmaefsky, 1990) and natural urine was quantified using the same assay. The assay was performed in triplicates. Only LB, sterile artificial urine and natural urine without bacterial culture was used as negative control for biofilm formation in each type of medium.

5.2.11 Quantification of components of biofilm matrix

eDNA, protein, EPS, and cells present in the matrix of weak and strong biofilms were quantified and normalized with OD_{600} (Wu and Xi, 2009; Madsen et al., 2015). 2 mL of 1:10 diluted culture (OD at 600 nm ~ 0.3) was inoculated in a 24-well plate and incubated at 37 ∘C for 48 h. The wells were decanted after 48 h and the biofilm was re-solubilized in 1 mL of 0.8% saline. The biofilm formed in 6-wells were pooled, SDS was added to final concentration of 0.01% and incubated at room temperature for 4 h at 150 rpm. Cell debris were removed by centrifugation at 5000× g for 5 min and the supernatant was passed through 0.2 μm cellulose acetate filter (Sartorious stedim Biotech Pvt. Ltd., Göttingen, Germany) and the filtered solution was used for eDNA and protein quantification. 1.5 mL of the pooled sample (before SDS treatment) was used for EPS quantification and live dead assay using flow cytometer.

5.2.11.1 eDNA quantification

The phenol-chloroform method was used for eDNA extraction and quantified using nanodrop (Thermo Fisher Scientific, Waltham, USA) (Wu and Xi, 2009). 500 µl of filtered solution was subjected to phenol-chloroform method to extract the extracellular DNA. Equal volumes of phenol, chloroform, and isoamyl alcohol mixture in ratio of 25:24:1 and filtered solution was centrifuged at 12,000× g for 10 min. The aqueous layer was separated and equal volume of chloroform and isoamyl alcohol in ratio of 24:1 was added, centrifuged at 12,000× g for 10 min. 1/10th volume of 3 M sodium acetate and 2.5 volume of absolute alcohol were added to the separated aqueous layer and stored at −20 ◦C overnight. Next day, this solution was centrifuged at 12,000× g for 10 min, the pellet was dissolved in 100 µl sterile distilled water and then absorbance was measured at 260 nm using nanodrop.

5.2.11.2 Extracellular protein quantification

The Bradford method was used for quantification of extracellular proteins present in biofilm matrix. 100 µl of Bradford reagent was added to 400 µl of filtered solution (mentioned above) and incubated at room temperature for 5 min and then absorbance was measured at 595 nm using a microtiter plate reader (Multiskan Go, Thermo Fisher Scientific, Waltham, USA).

5.2.11.3 Exopolysaccharide (EPS) quantification

EPS present in the matrix was quantified using Congo red binding assay (Madsen et al., 2015). Briefly, Congo red was added to the final concentration of 40 µg/mL in 1 mL of homogenate and incubated at 37 ◦C for 2 h in shaking conditions. The solution was centrifuged to pellet down the cells, and the absorbance of the supernatant was measured at 490 nm. 1 mL of 0.8% saline with Congo red was used as the reference. The percentage of Congo red bound to the cells was calculated as follows: % bound Congo red = $100 - (OD_{490}$ of test supernatant $\times 100)/OD\ OD_{490}$ of reference).

5.2.11.4 Live Dead assay

BacLight™ kit L7012 (Thermo Fisher Scientific, Waltham, MA, USA) was used to perform the live dead assay. 2 µl of syto9 (1:5 dilution) and PI mixture

in 1:1 ratio was added to 300 µl of solubilized biofilm solution (without SDS treatment) and subjected to flow cytometry (Becton Dickinson FACSCalibur, New Jersey, United States). 300 µl of solution stained individually with syto9 and PI and 300 µl of unstained culture were used as controls to eliminate the auto-fluorescence/background of the sample in flow cytometry. Double positive cells (syto9+ and PI+) contribute to the number of dead cells (total PI+). Double positive cells were considered as dead cells because PI has displaced syto9 as the membrane of these cells is damaged/compromised (dying cells) (Accurate Assessment of Microbial Viability by Flow Cytometry 2011).

5.2.11.5 Resazurin assay

In Resazurin assay, 0.015 mg/mL stock solution in 0.8% saline was used (Peeters et al., 2008). Briefly, 250 µl of 1:10 diluted culture was inoculated in a 96-well microtiter plate and incubated at 37 ∘C for 24 h. The unbound cells were washed off with distilled water and 20 µl of resazurin dye (HiMedia Laboratories Pvt. Ltd., Mumbai, India) diluted in 100 µl of 0.8% saline and was added in each well and incubated at 37 ∘C for 60 min. The fluorescence was measured at 530/590 nm excitation/emission wavelengths using the synergy HTmicroplate reader (BioTek instruments, Winooski, VT, USA).

5.2.12 Time bound live dead assay

Live dead assay was performed at 6, 18, and 24 h to study the change in the ratio of live and dead cells in weak and strong biofilm at various time points. Briefly, 25 µl of overnight grown culture (1:10 dilution of O.D at 600 nm ~ 0.3) was added to 225 µl of sterile LB in a sterile black opaque walled 96-well microtiter plate to reduce fluorescent signal crosstalk and background (Laxbro Bio-Medical Aids pvt. Ltd., India). The plate was then incubated at 37 ∘C for 6, 18, and 24 h. The assay was performed in triplicates. Only LB without bacterial culture was used as negative control for biofilm formation. After respective time points, the unbound cells were washed off using 0.8% normal saline and the biofilm was solubilized in 100 µl of 0.8% saline. Staining and detection of the absorbance was done as per the protocol given in the kit manual. Briefly, BacLight kit L7012 A concentrated dye solution containing equal volume of syto9 and PI (15 µl each) (Baclight kit L7012) in 5.5 mL of autoclaved

molecular grade water was prepared and 100 µl of this dye solution was added in each well. Proper mixing with pipetting was done and the plate was incubated at room temperature for 15 min. After incubation, fluorescence intensity was measured using the synergy HTmicroplate reader (BioTek instruments, Winooski, USA). The excitation/emission spectrum used to detect syto9 and PI stained cells was 485/530 nm and 485/630 nm, respectively. Measure of live and dead cells was calculated in term of intensity units (IU) detected of syto9 and PI. The experiment was performed in triplicates.

5.2.13 Inhibition assay

 Inhibition assay was performed to validate the role of different biofilm matrix components (Tetz et al., 2009). Briefly, 25 µl of overnight grown culture (OD at 600 nm ~ 0.3) was added to 225 µl of sterile LB in a sterile 96-well flat bottom microtiter plate (Laxbro Bio-Medical Aids pvt. Ltd., Pune, India) and incubated at 37 ºC for 24 h. The assay was performed in triplicates and only LB was used as the negative control. After 24 h, the unbound cells were washed off twice with 0.8% saline and 100 µg/mL of DNase I, RNase A, and Proteinase K enzyme solution was added separately in triplicates and further incubated at 37 ºC for 24 h. A set of wells containing 25 µl of overnight grown culture (OD at 600 nm ~ 0.3) and 225 µl LB only without addition of any enzyme were used as controls. After 24 h, the enzyme solution and unbound cells were washed off twice with 0.8% saline and crystal violet assay was performed to quantify the amount of biofilm. Paired t-test was applied to validate the decrease in biofilm formation upon enzymatic treatment statistically.

5.2.14 Addition assay

Addition assay was performed to validate the role of different biofilm matrix components (Harmsen et al., 2010). Briefly, 25 µl of overnight grown culture (OD at 600 nm ~ 0.3) was added to 225 µl of sterile LB in a sterile 96-well flat bottom microtiter plate (Laxbro Bio-Medical Aids pvt. Ltd., Pune, India). *Kp* cell extracted DNA and protein was added separately to the final concentration of 3 µg/mL in the wells. The 96-well plate was then incubated at 37 ◦C for 24 h. The assay was performed in triplicates and wells containing only LB were

used as the negative control. A set of wells containing 25 µl of overnight grown culture (OD at 600 nm ~ 0.3) and 225 µl LB only without addition of DNA and Protein were used as controls. After 24 h, the unbound cells were washed off twice with 0.8% saline and crystal violet assay was performed to quantify the amount of biofilm. Paired t-test was applied to validate the change in biofilm formation upon addition of DNA or proteins statistically.

5.2.15 Microscopy of strong and weak biofilms

5.2.15.1 CLSM

Biofilms formed by three weak and three strong isolates on glass coverslips were subjected to CLSM after 48 h. 5 mL of 1:10 diluted culture (OD at 600 nm ~ 0.3) was inoculated in a 6-well plate containing sterile glass coverslips of 22 mm diameter. The biofilm was allowed to form for 48 h at 37 ∘C. The unbound cells were washed off with 0.8% saline and the cells embedded in the biofilm were stained with syto9 and PI for 10 min. Excess stain was washed away with 0.8% saline and the coverslip was mounted for CLSM. Carl Ziess CLSM 780 microscope equipped with detectors and filter sets for simultaneous monitoring of Syto9 (green) (multi argon laser, 488 nm excitation, emission spectra 492–525 nm) and PI (red) (DPSS laser, 561 nm excitation, emission spectra 563-652 nm) fluorescence was used to study the arrangements of live and dead cells embedded in the biofilm matrix. Visualization of 3D structure was done using Z-stack mode of CLSM. Large section images were produced by tile scanning of strong and weak biofilms formed by all six biofilm producers. Images were analysed using ImageJ and Zen Zeiss microscope software. The intensity units of syto9 and PI in each slice from top to bottom of the Z-stack was calculated using ImageJ for all isolates. Number of live and dead cells of all isolates was calculated from the tile images using ImageJ. Area of 1000 × 1000 pixel in tile images was used as a region of interest (ROI) to calculate the ratio of live and dead cells for all isolates.

Biofilm was formed on 13 mm piece of silicone coated latex catheter as described above and FEG-SEM (Nova NanoSEM 450, FEI Ltd., Hillsboro, OR, USA) was performed for strong and weak biofilms formed on silicone-coated latex catheter after 24 h. SEM scanning was done at room temperature in environmental mode.

5.2.16 Cell adhesion assay

Cell adhesion assay was performed to evaluate the adhesion ability of weak and strong biofilm producers. 5 mL of 1:10 diluted culture (OD at 600 nm ~ 0.3) was inoculated in a 6-well plate containing sterile coverslips of 22 mm diameter. Cells were allowed to adhere for 4 h at 37 ∘C. The unbound cells were then washed off with 0.8% saline and cells adhered on coverslip were subjected to gram staining followed by light microscopy (Magnüs MLM). The number of cells adhered on the coverslip were calculated for 10 fields at 100× magnification using ImageJ for all six isolates.

5.2.17 Statistical analysis

All assays were performed in triplicates and standard deviation (SD) values were calculated. Nonparametric paired and unpaired student's t-test were performed using Prism 8.0 Software (GraphPad, San Diego, USA) to statistically evaluate the differences obtained. p-value of < 0.05 was considered statistically significant.

5.3 Results

Study of CPS, EPS, string formation, rmpA

5.3.1 Quantification of CPS

Wide range of CPS production among isolates was observed (5.2 µg CPS/mg protein to 116.38 µg CPS/mg protein as shown in figure 5.1. M34 was found to produce the highest amount of CPS, 116.38 µg CPS /mg protein; production of CPS was the lowest in M10, 5.2 µg CPS/mg protein.
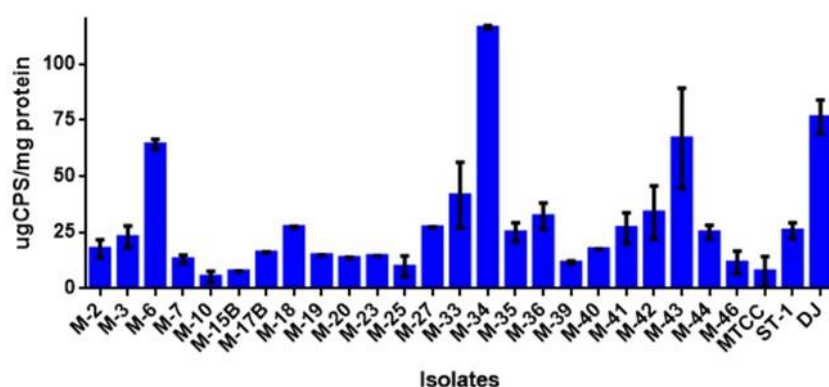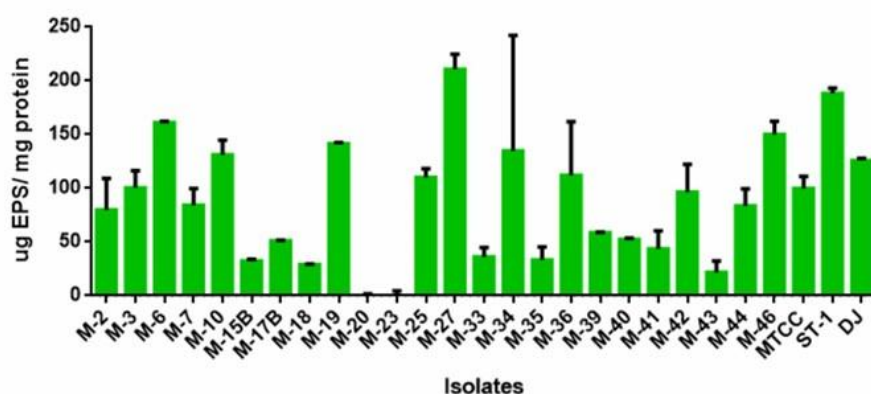
Figure 5.1 Quantification of CPS. Wide range of CPS production by uro-pathogenic *Klebsiella* isolates is shown. The amount of CPS production exhibited a wide range from 116.38 µg CPS/mg protein in M34 to 5.2 µg CPS/mg protein in M10.

5.3.2 Quantification of EPS

A wide range of EPS production was observed among the isolates as shown in figure 5.2. M27 was found to produce the highest amount of EPS 210.79 µg EPS /mg protein. M20 and M23 were not found to produce EPS (0 µg EPS/mg protein).

Figure 5.2 Quantification of EPS. Wide range of EPS production by uro-pathogenic *Klebsiella* isolates is shown. The amount of EPS production exhibited a wide range from no EPS (0 µg EPS/mg protein) was produced in M20 and M23 to 210.79 µg EPS/mg protein (highest) by M27.

5.3.3 Correlation between CPS and EPS

Figure 5.3 shows the correlation between CPS and EPS production by isolates. Value of Pearson's correlation co-efficient (r) was found to be 0.20. Value of r and the scatter plot (figure 5.3) correlating CPS and EPS indicate no correlation between CPS and EPS production by isolates was found.

5.3.4 Frequency distribution of CPS and EPS

The frequency distribution analysis suggested that though the isolates showed a wide range of CPS production and the maximum CPS production found was 116.38 µg CPS /mg protein, majority of the isolates have produced CPS between the range of 10 to 40 µg/mg protein (figure 5.4A). In case of EPS, the frequency distribution indicates that production of EPS in majority of the isolates was similar with average EPS production of 84 µg EPS /mg protein (figure 5.4B).

5.3.5 Detection of string phenotype

All the isolates were grown as off-white colored (pearl-like) mucoid colonies on blood agar. Only M20, the isolate with low CPS and no EPS was found to be string positive with >5 mm string (figure 5.5). Rest of the isolates did not form string >5 mm and were found to be string negative.
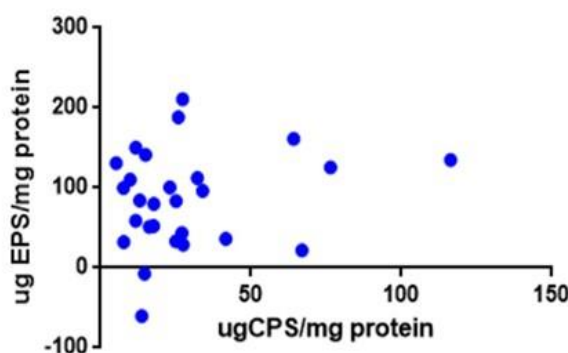

Figure 5.3 Correlation between CPS and EPS. Correlation between CPS and EPS was analysed by the scatter plot. Each dot in the plot shows amount of CPS and EPS produced by each isolate. The scatter plot indicates no correlation between the production of CPS and EPS. Pearson's Correlation test was performed using Prism 8 GraphPad.
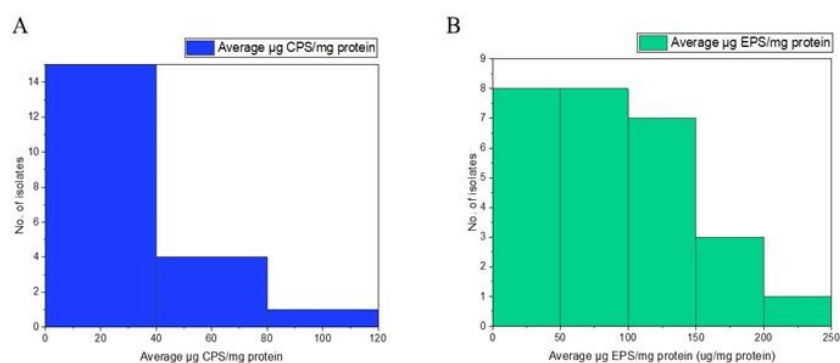
Figure 5.4 Frequency distribution of CPS and EPS. (A) Frequency distribution of CPS produced by the isolates, which indicates that majority of the isolates have produced CPS between the range of 10 to 40 µg/mg protein. (B) Frequency distribution of EPS produced by the isolates, which indicates that the majority of the isolates produced similar amount of EPS with an average production of 84 µg EPS /mg protein. The distribution was analysed using frequency distribution using Origin Pro 2019
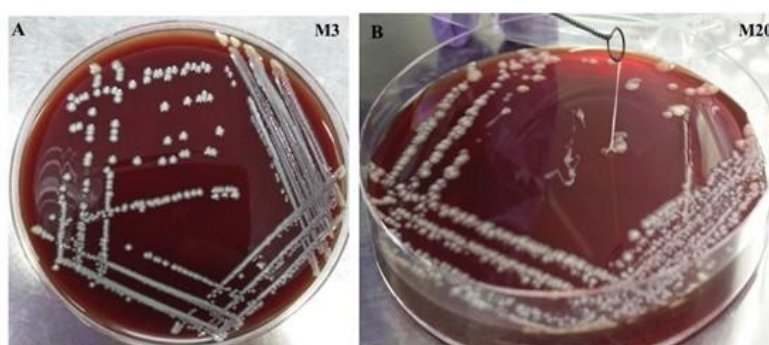

Figure 5.5 Detection of string phenotype. (A) Representative image of off-white colored (pearl-like) mucoid colonies of *Klebsiella* isolate (M3) grown on blood agar. (B) >5 mm string formed by isolate M20, string positive isolate.

5.3.6 Study of *rmpA*

5.3.6.1 Detection of rmpA using PCR

rmpA, a virulence gene responsible for mucoid phenotype, was amplified only in five isolates M39, M41, M42, M43, MTCC with amplicon size of 536 bp (figure 5.6). Rest of the isolates were not found to carry *rmpA.*

<u>*5.3.6.2 Study of rmpA gene expression using qRT-PCR*</u>

Isolated RNA without gDNA contamination is showed in figure 5.7A. Figure 5.7B shows the fold change of *rmpA* expression in *rmpA* positive isolates. M39 showed highest overexpression of *rmpA* (3315 folds) compared to MTCC strain. Whereas, M41, M42 and M43 showed 4.8 folds 4.05 and 1.72 folds overexpression of *rmpA* compared to MTCC strain, respectively.
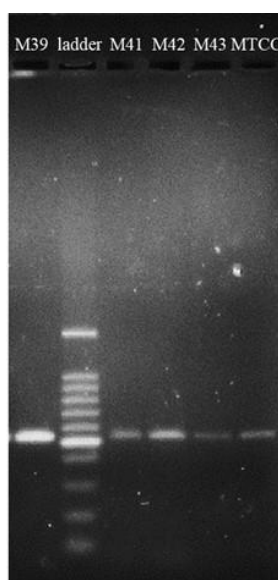

Figure 5.6 Presence of *rmpA*. Agarose (1%) gel electrophoresis of *rmpA* gene amplified using PCR along with 1 kb ladder. *rmpA* was amplified in isolates M39, M41, M42, M43 and MTCC with an amplicon size of 536 bp. Name of the isolates are shown on the top of each lane of the gel image.
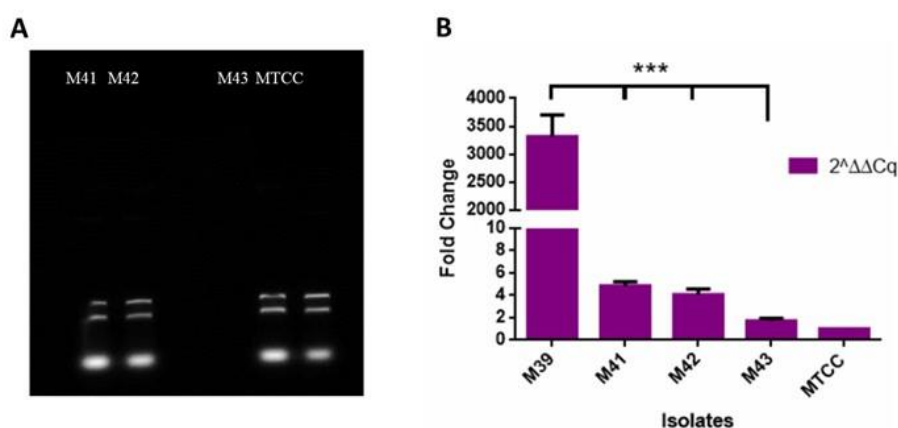

Figure 5.7 Study of *rmpA* gene expression using qRT-PCR. (A) RNA isolation for study of *rmpA* expression. 2% agarose gel electrophoresis of isolated RNA from M41, M42, M43 and MTCC. Name of the isolates are shown on the top of each lane of the

gel image. (B) fold-change of *rmpA* gene of isolated M39, M41, M42, M43 and MTCC. Fold-change of gene-expression is calculated from C_q/C_t value of qRT-PCR. MTCC *Kp* strain 39 was used as reference isolate for calculating fold change. *rpoB* (housekeeping gene) was used as the internal control for study of relative gene expression.

5.3.7 Phagocytosis assay

5.3.7.1 Selection of isolates for phagocytosis assay and determination of K-type using wzi sequencing

To determine the role of virulence factors like amount of CPS and EPS, string phenotype and expression of *rmpA* in resistance of phagocytosis, we selected isolates with highest and lowest amount of CPS and EPS, overexpression of *rmpA* as well as string positive isolates as showed in table 5.9. Serotype/K-type of the above-mentioned isolates was determined using *wzi* sequencing. Isolates with K2 and non-K2 types were included for the study, which would help us to evaluate the role of serotype in resistance to phagocytosis.

570 bp amplicon of *wzi* gene was amplified in isolates M10, M20, M27, M34 and M43 (figure 5.8). K-type of M10, M20, M27, M34 and M43 were found to be K23, K39, K2, K2 and K10, respectively.

Table 5.9 Isolates selected for phagocytosis assay and their criteria.

Isolate	Amount of CPS	Amount of EPS	String test	Expression of *rmpA*	K-type
M10	+	++	--	--	K23
M20	+	--	+	--	K39
M27	++	+++	--	--	K2
M34	+++	++	--	--	K2
M39	+	++		+++	K74
M43	++	+	--	+	K10

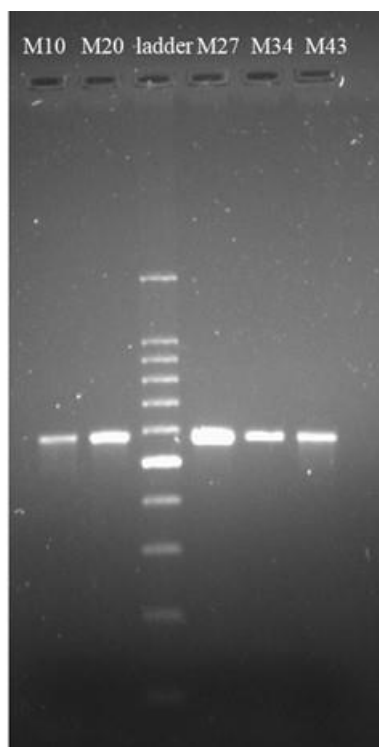+++ Highest; ++ high-moderate; + Very low; -- Not present/not produced/ negative

Figure 5.8 Amplification of *wzi* for determination of K-type. Agarose (1%) gel electrophoresis of *wzi* gene amplified using PCR along with 1 kb ladder. *wzi* was amplified in isolates M10, M20, M27, M34 and M43. Name of the isolates are shown on the top of each lane of the gel image.

5.3.7.2 FITC-labelling

FITC-labelling of all above selected isolates was performed. FITC-labelled isolates were observed as green colored short-rods during fluorescent microscopy.

5.3.7.3 Flow-cytometric analysis of phagocytosis assay

During a pilot experiment, the tubes were incubated at different time points. However, maximum phagocytosis was observed at 15 minutes and after 15 minutes (in tubes with 30 and 60 minutes) no further increase or change in amount of phagocytosis was observed. Therefore, further all the experiments were performed at 15 minutes incubation. Figure 5.9 shows histograms of observed phagocytosis of FITC-labelled *Kp* isolates by neutrophils. Among all the isolates, the least amount of phagocytosis was observed in case of the only string positive isolate, M20 (56.7%) followed by M10 (68.8%) and M27

(69.7%) and M39 (74.5%). Highest phagocytosis (85.5%) was observed in M43 (high CPS, string negative) followed by M34 (highest CPS, string negative) (80.3%). Statistical signifcanse of difference in %phagocytosis between M20 and all other isolates is shown in figure 5.9. Hence, %phagocytosis observed among the isolates (n=6) was **M20**(String positive)**<M10** (lowest CPS)**<M27** (highest EPS)**<M39** (Highest expression of *rmpA*)**<M34** (highest CPS) **<M43** (High CPS + moderate overexpression of *rmpA*).
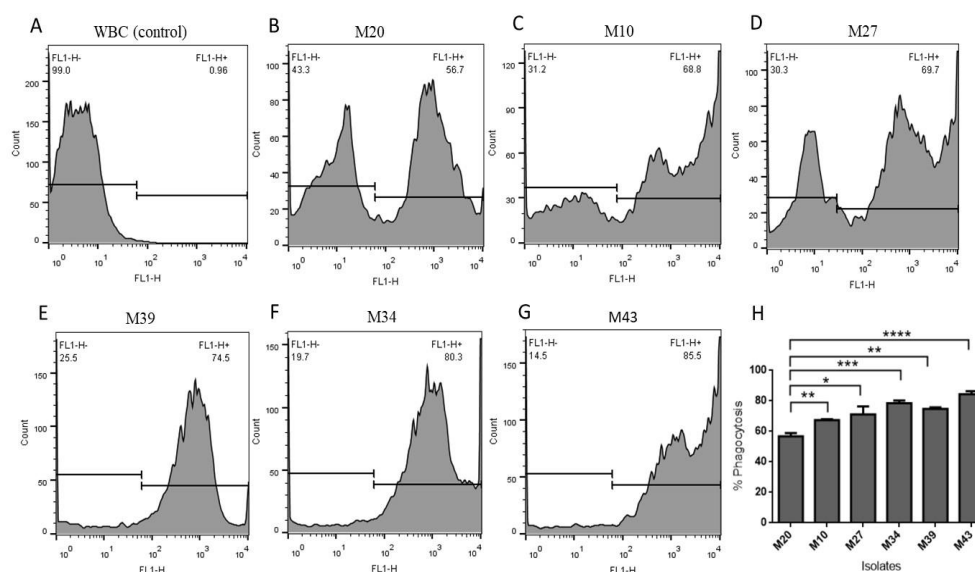

Figure 5.9 Flow-cytometric analysis of phagocytosis assay. The representative histograms show phagocytosis of FITC-labelled *Kp* isolates into neutrophils of donor 1. (A) Uninfected (not infected using FITC-labelled *Kp*) and unlabeled WBCs were used as control, (B) M20, (C) M10, (D) M27, (E) M39, (F) M34 and (G) M43. The part of histogram after the cut-off line shows number of neutrophils with ingested FITC (Green) labelled *Kp* (phagocytosed bacteria). (H) %phagocytosis of n=6 isolates; The error bars indicate standard deviation between three independent experiments. $1*10^6$ WBCs were incubated for 15 minutes with $4*10^7$ CFU/ml FITC-labelled bacteria individually to establish infection. Y axis shows cell count and X-axis shows green fluorescence of FITC (FL1-H) plot. Population was gated to selectively include granulocytes only. Cut-off was made using control to avoid background fluorescence of the cells. Same cut-off was used to analyze phagocytosis in all the isolates. The analysis of FACS data was done using FlowJo_v10. Statistical analysis was performed by the unpaired t-test using Prism 8 GraphPad. * $p < 0.05$; ** $p < 0.01$, *** $p < 0.001$, **** $p < 0.0001$.

5.3.7.4 Visualization of phagocytosis using Fluorescence microscopy and CLSM

During fluorescence microscopy, FITC-labelled bacteria localized inside neutrophils/PMN were observed in green color. Bacteria not localized inside neutrophils/phagocytosed were observed in orange color (figure 5.10A). CLSM further confirmed the occurrence of phagocytosis event and location of FITC-labelled *Kp* inside neutrophils (figure 5.10B). FITC-labelled *Kp* bacterial cells (green) were clearly observed to be phagocytosed and localized inside polymorphonuclear neutrophils (red ,EtBr stained).
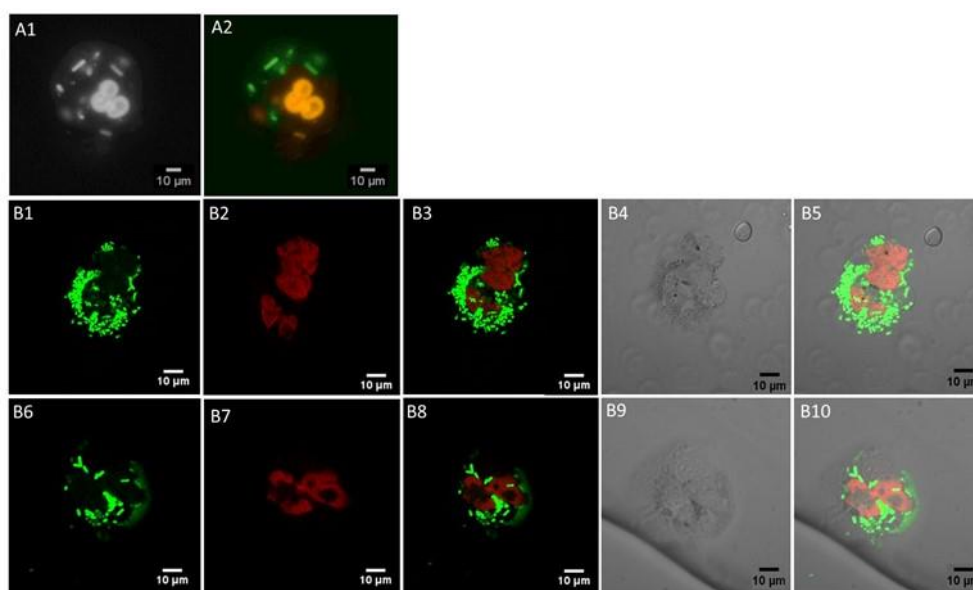

Figure 5.10 Visualization of phagocytosis using fluorescence microscopy and CLSM. The figure shows micrographs of phagocytosis assay using fluorescence and confocal microscopy. (A) Representative images of fluorescence microscopy (A1) monochromatic (A2) Composite/colored image with merged channels (red and green) of fluorescence microscopy of FITC-labelled bacterial (green, short-rods) isolate M34 phagocytosed by neutrophils of donor 1 (orange, polymorphonuclear cell). 3 orange colored rod-shaped bacteria observed were the extracellular bacteria counter stained by EtBr; these bacteria are not localized inside the neutrophils (phagocytosed). (B1-B5) Confocal microscopy of FITC-labelled *Kp* isolate M43 phagocytosed by neutrophils. (B1) FITC-labelled *Kp* isolate (green). (B2) EtBr stained neutrophils (red, chambered cell) (B3) merged image of channel B1 (green) and B2 (red) where FITC labelled bacteria (green) was phagocytosed (localized inside) the neutrophils (red). (B4)

Differential interference contrast (DIC) image of the same field. (B5) Composite image of all filters B1-B4. Similarly, (B6-B10) Confocal microscopy of FITC-labelled *Kp* isolate M20 phagocytosed by neutrophils. (B6) FITC-labelled *Kp* isolate (green). (B7) EtBr stained neutrophils (red, chambered cell) (B8) merged image of channel B6 (green) and B7 (red). (B9) DIC image of the same field. (B10) Composite image of all filters B6-B9. The scale bar in the image shows measure of 10 μm. $1*10^6$ WBCs were incubated for 15 minutes with $4*10^7$ CFU/ml FITC-labelled *Kp* isolates individually to establish infection.

Study of Biofilm

5.3.8 Biofilm Formation by uro-pathogenic *Kp* isolates

Biofilm formation by all the clinical isolates (n = 28) was studied using crystal violet assay in a 96-well polystyrene plate and categorized as per their biofilm forming ability (figure 5.11A). Majority of the isolates were able to form a strong or moderate type of biofilm. A non-pathogenic microbial type culture collection (MTCC) strain 39 of *Kp* also formed moderate level of biofilm. Among all the collected isolates 43%, 43%, and 14% were strong, moderate, and weak biofilm producers, respectively (figure 5.11A). From 28 biofilm producer isolates of different categories, three weak, M-20,23, and 25 and three strong (M-10,27, and 34) biofilm producers were selected randomly for further study. The average growth rate of these selected isolates measured was 0.841 ± 0.03/h (figure 5.11B). MLST types of M-20,23,25,10,27, and 34 are ST2943, ST10, ST1087, ST2491, ST1715, and ST38, respectively. Biofilm formation by these six isolates on various catheters (figure 5.11C) in presence of different media (figure 5.11D,E) was investigated. In case of weak biofilm, significant difference in biofilm formation between latex and silicone coated latex, as well as silicone catheters was observed (p < 0.0001) (figure 5.11C). The difference in biofilm formation between silicone coated latex and silicone catheters was also significant with p < 0.001 in weak biofilms. In case of strong biofilm, significant difference between latex and silicone (p < 0.01); latex and silicone-coated latex (p < 0.05) was observed. No significant difference between silicone-coated latex and silicone was observed in case of strong biofilm. When biofilm formation was studied on two types of catheters, in the presence of

different media, significant increase in biofilm formation was observed in case of natural urine as compared to Luria-Bertani (LB) broth and artificial urine on silicone-coated latex catheter (figure 5.11D) and silicone catheter (figure 5.11E) (p-value shown in figures). Hence, the biofilm formation was lowest on silicone catheters followed by silicone-coated latex and latex catheters. In the presence of different media, the biofilm formation was highest in natural urine followed by LB and artificial urine.
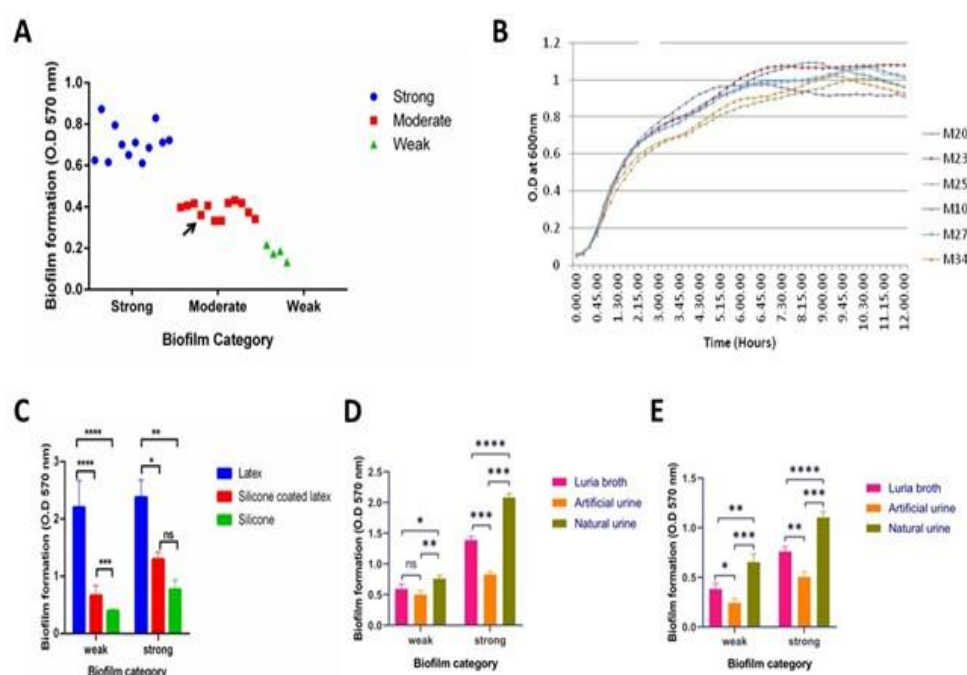

Figure 5.11 Biofilm formation by uro-pathogenic *Kp* isolates. (A) Quantification and categorization of biofilm producer isolates (n = 28). Black arrow indicates biofilm formation by MTCC *Kp* 39. (B) Growth curve of weak (M20,M23,M25) and strong (M10,M27,M34) biofilm producers at 15 min interval till 12 h. (C) Biofilm formed by strong (M-10,27,34) and weak (M20,M23,M25) biofilm producers on latex, silicone-coated latex and silicone catheters. Biofilm formed in the presence of LB broth, artificial urine, and natural urine on (D) silicone-coated latex and (E) silicone catheters. Statistical analysis was performed by the unpaired t-test using Prism 8 GraphPad. * $p < 0.05$; ** $p < 0.01$, *** $p < 0.001$, **** $p < 0.0001$, ns $p > 0.05$**.**

5.3.9 Components of strong and weak biofilm matrix

The average amount of eDNA quantified from weak biofilm matrix (344.5 µg/OD600) was lower when compared to eDNA from strong biofilm matrix (1673 µg/OD600), which was significantly higher ($p < 0.01$) (figure 5.12A).

The average amount of extracellular protein present in weak and strong biofilm matrix was 197.1 and 584.4 µg/OD600, respectively (figure 5.12B). Exopolysaccharides (EPS) obtained in weak and strong biofilm matrix was 46.31% and 52.38%, respectively (figure 5.12C). The measure of live cells in biofilm was obtained using resazurin assay. Average fluorescence units (FU) obtained in weak and strong biofilms were 2658 and 1381 FU, respectively (figure 5.12D). Significantly less number of live cells were found in strong biofilm than weak biofilm ($p < 0.05$). Previously, it has been reported that the live cells measured by resazurin assay and estimated CFU present in biofilm show negligible amount of variation. Hence, we have performed resazurin assay for quantification of live and dead cells present in the biofilm (Peeters et al., 2008).

The number of dead cells present in weak and strong biofilm was evaluated using flow- cytometry analysis after 48 h. 23% of dead cells (Propidium iodide (PI) positive cells) were observed in weak biofilm as compared to 65% in strong biofilm. This indicates that more number of dead cells were present in strong biofilm than weak biofilm with $p < 0.01$ (figure 5.12E).

Time bound live dead assay was done at 6, 18, and 24 h to see the live dead ratio in weak and strong biofilms. In case of strong biofilm, cell death (intensity of PI) was observed to be increased at 18 h (105 ± 9 IU) than at 6 h (4.4 ± 0.5 IU) and maximum intensity of PI was measured at 24 h (194 ± 10 IU). Whereas, in case of weak biofilm cell death (intensity of PI) was high at 18 h (37 ± 1 IU) than at 6 h (3.4 ± 0.3). However, in 24 h, intensity of PI was significantly lesser (47 ± 5 IU) compared to that of the strong biofilm (194 ± 10 IU). (figure 5.12F). Though the growth rate of all the isolates are similar, cell death was found to be increased with the time only in strong biofilms.

To summarize, significantly higher amount of eDNA ($p < 0.001$), protein ($p < 0.001$), EPS ($p < 0.05$), and dead cells ($p < 0.05$) were observed in strong biofilms than in weak biofilms.

5.3.10 Inhibition and Addition Assay

To further validate the role of different matrix components in biofilm formation, we performed inhibition and addition assays. In case of strong biofilm, significant reduction in biofilm was observed after treating the biofilm with DNase I (46.62%) (figure 5.13A), RNase A (48.12%) (figure 5.13B), and Proteinase K (72.9%) (figure 5.13C). In case of weak biofilm, biofilm was reduced by 26.19%, 0.1%, and 29.4% upon DNase I (figure 5.13A), RNase A (figure 5.13B), and Proteinase K (figure 5.13C) treatment, respectively. However, exogenous addition of *Kp* cell extracted DNA and protein to both weak and strong biofilms did not show any significant change in biofilm formation (figure 5.13D).
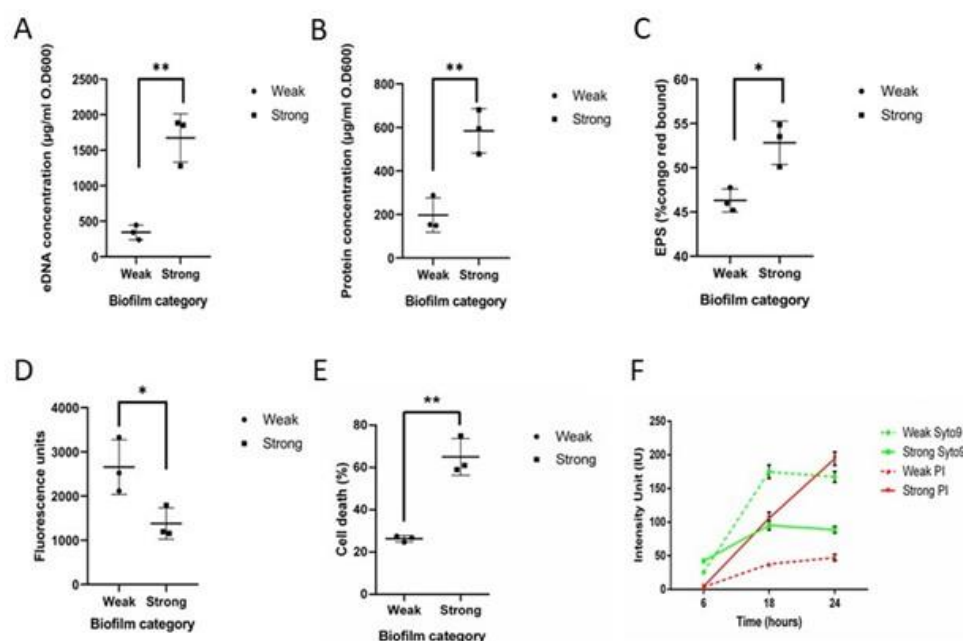

Figure 5.12. Components of strong and weak biofilm matrix. Amount of various components present in biofilm matrix were quantified. (A) eDNA (B) Protein (C) Total exopolysaccharides (EPS) (D) The measure of live cells in biofilm using resazurin assay in terms of average fluorescence unit. (E) Flow-cytometry analysis of live dead assay using BacLight kit (syto9 and propidium iodide (PI)). (F) Intensity of live cells stained with syto9 (green) and dead cells stained with PI (red) measured at 6, 18, and 24 h in weak (dotted line) and strong (solid line) biofilms by time bound live dead assay. Quantification was done from biofilms formed by three weak (M-20,23,25) and

three strong (M-10,27,34) biofilm producers. Statistical analysis was performed by the unpaired t-test using Prism GraphPad. *, p < 0.05; **, p < 0.01.
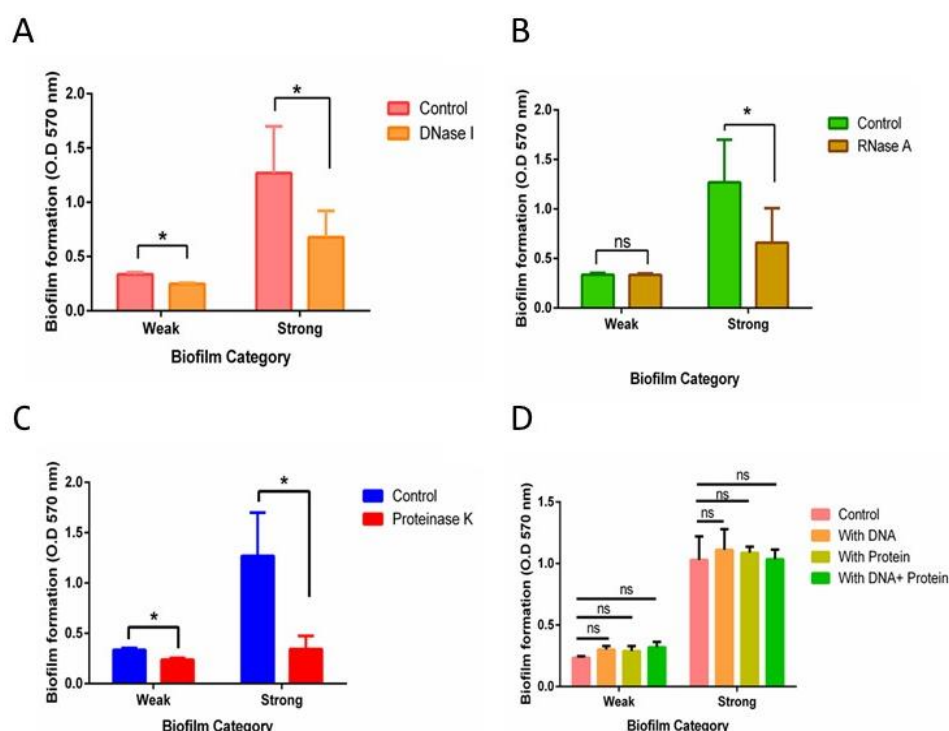

Figure 5.13. Inhibition and addition assay. Inhibition assay was performed to validate the role of eDNA, RNA (Ribonucleic acid), and protein in biofilm formation. Quantification of weak and strong biofilms after the treatment of (A) DNase I (B) RNase A, and (C) Proteinase-K. Biofilm formed without the treatment of enzymes was used as control. Concentration of all three enzymes used for the treatment was 100 µg/ml. For addition assay, *Kp* cell extracted DNA and proteins were added separately and both together at 0 h and biofilm was allowed to form for 24 h at 37 ∘C. (D) Quantification of weak and strong biofilm formed after addition assay. Concentration of DNA and protein used for the treatment was 3 µg/ml. Statistical analysis was performed by the unpaired t-test using Prism GraphPad. *, p < 0.05.

5.3.11 Microscopy of weak and strong biofilm

To characterize the weak and strong biofilms, confocal laser scanning microscopy (CLSM), light microscopy, and field emission gun scanning electron microscopy (FEG-SEM) were performed for three weak (M-20,23,25) and three strong (M-10,27,34) isolates. To visualize 3D structure of live and dead cells embedded inside the biofilm matrix and to further evaluate the huge amount of cell death observed in strong biofilms, CLSM was performed.

Distinct differences in the biofilm structure and thickness were observed between strong and weak biofilms formed by all six biofilm producers in CLSM (figure 5.14). Orthogonal views of weak and strong biofilms show differences in thickness and arrangement of live and dead cells in the biofilm matrix. Weak biofilm (figure 5.14A) was observed to be sparsely packed with more numbers of live cells whereas strong biofilm was densely populated with more numbers of dead cells compared to live cells (figure 5.14 4B). YZ and XZ planes of figure 5.14A,B also give information about the difference in the thickness of weak and strong biofilms. figure 5.14C,D indicates the measure of live and dead cells based on the intensity units. It was observed that in weak biofilm, the number of live cells increased, and dead cells decreased with the increase in the depth (figure 5.14C). In strong biofilms, the number of dead cells increased, and live cells decreased with increase in the depth (figure 5.14D). It was also observed that the thickness of weak biofilm was observed to be only 19 slices thick whereas, strong biofilm was observed to be expanded up to 40 slices with the uniform slice interval of 0.36 μm. This also indicates a significant difference in the thickness of weak (7 ± 2 μm) and strong biofilms (14 ± 1 μm). Tile image of weak biofilm showed the presence of less number of dead cells and more number of live cells (figure 5.14E). On other hand, tile image of strong biofilm showed a large number of dead cells and very less number of live cells (figure 5.14F). The number of live and dead cells in weak biofilm were 260 ± 33 and 60 ± 11, respectively in the area of 1000×1000 pixel (region of interest (ROI)) of the tile image. The number of live and dead cells in strong biofilm are 45 ± 6 and 369 ± 42 cells, respectively (figure 5.14G). The difference in cell death

between flow cytometry and CLSM is due to the difference in the assays. Interestingly, 3D structure of strong biofilm showed pockets of live cells embedded within the thick layers of dead cells.

To study the differences in adhesion capacity, three weak and three strong biofilm producers were subjected to cell adhesion assay followed by light microscopy. Very few Gram-negative rods in light microscopy were observed to be adhered in weak biofilm producers (figure 5.15A). Conversely, large number of cells were observed to be adhered in strong biofilm (figure 5.15B) during early biofilm stage (4 h). Number of cells adhered to the coverslip after

4 h of biofilm formation were 125 ± 18 and 542 ± 20 in weak and strong biofilms (figure 5.15C). This indicates that adhesion capacity of strong biofilm producers is higher than the weak biofilm producers.

FEG-SEM was performed to investigate the differences in the structure of weak and strong biofilms formed on silicone-coated latex catheters. FEG-SEM micrographs of weak biofilms showed very less number of cells embedded in cloud like EPS. It also suggests the presence of micro-channel like structures in the network of exo-polymeric matrix (figure 5.16A,C,E). On other hand, the strong biofilm micrographs showed higher number of interconnected cells embedded in densely populated and abundant extracellular matrix (figure 5.16B,D,F).
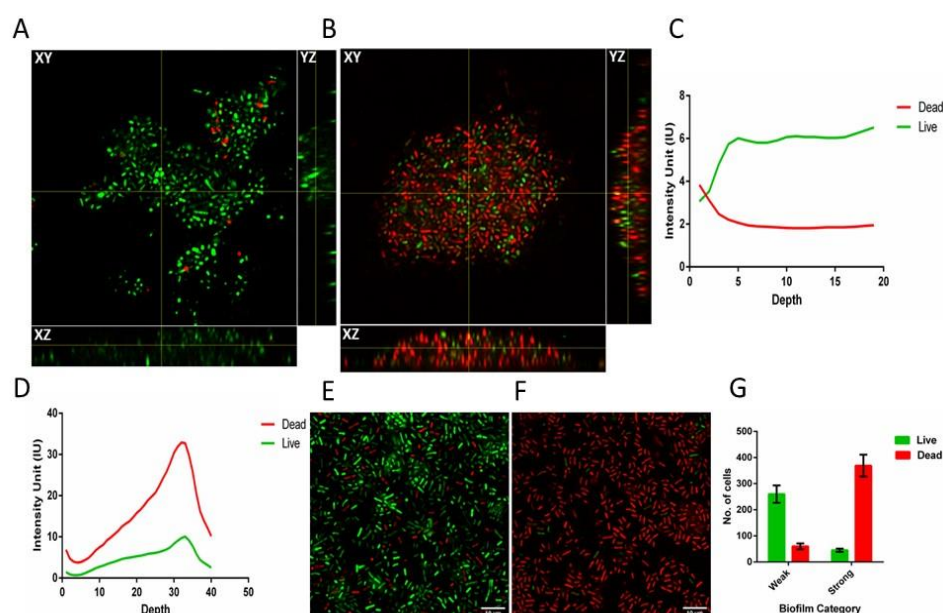

Figure 5.14 Confocal laser scanning microscopy (CLSM) of weak and strong biofilms. Representative orthogonal view of the Z-stack (A) weak and (B) strong biofilms are shown with XY, YZ, and XZ planes. Intensity of syto9 (green) and PI (red) was measured across the depth of the Z-stack and live dead ratio was estimated based on intensity units (IU) for both weak(C) and strong (D) biofilm. Representative tile images of weak (E) and strong (F) biofilm shows the distribution of live (green) and dead (red) cells in the biofilm matrix. Array of multiple images is presented as a single tile image. (G) Quantification of number of live and dead cells present in weak and strong biofilm. Images were analysed using ImageJ2 and Zen Zeiss microscope software.
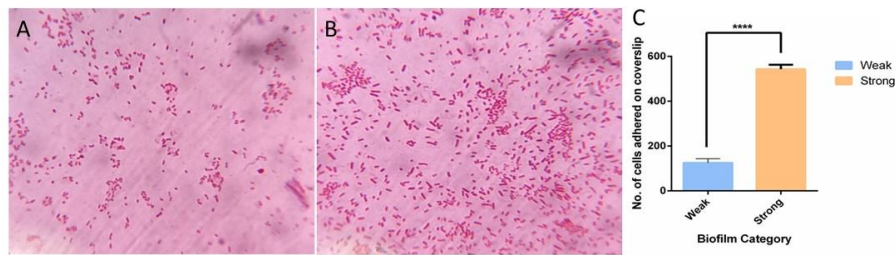
Figure 5.15 Adhesion assay of weak and strong biofilms. Representative light microscopy images of (A) weak and (B) strong biofilm producers adhered to the coverslip after 4 h are shown. (C) Average number of cells adhered in weak and strong biofilms after 4 h of cell adhesion assay. ImageJ2 was used to analyse the images. ****, $p < 0.0001$.
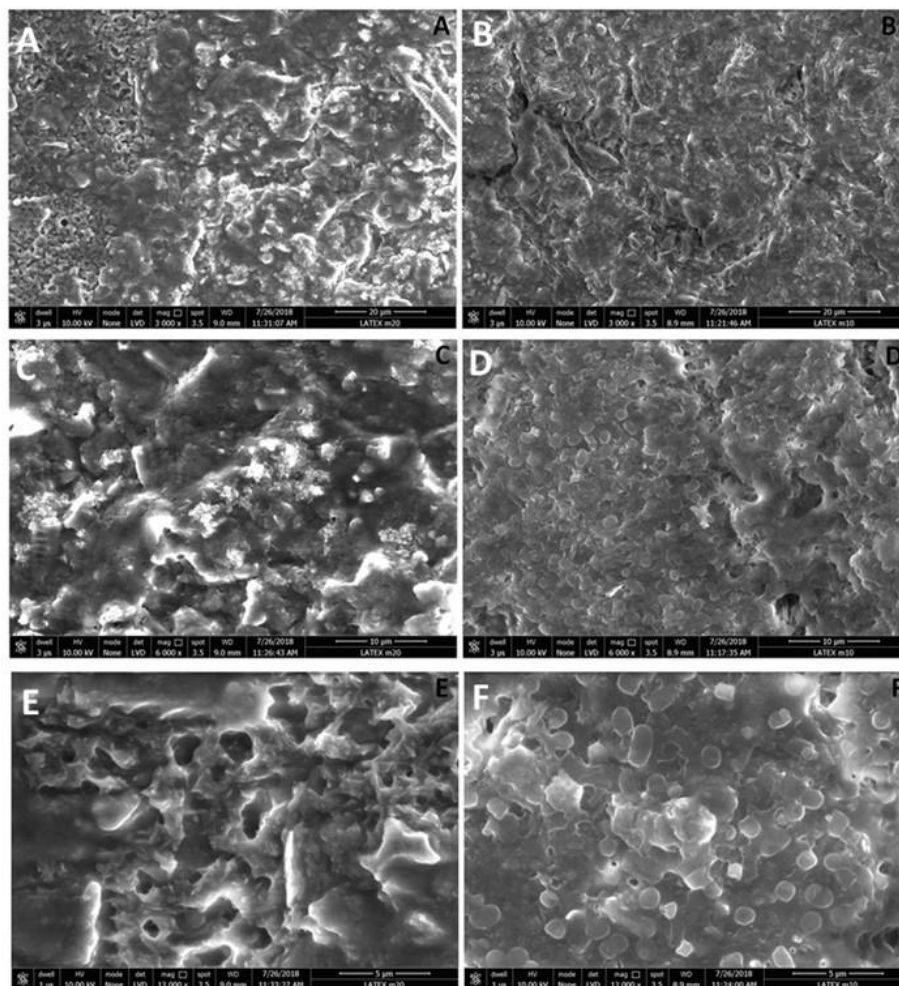

Figure 5.16 FEG-SEM of weak and strong biofilms. FEG-SEM of weak and strong biofilms formed on 13mm long piece of silicone-coated latex catheter. SEM micrographs of weak biofilm (A,C,E) and strong biofilm (B,D,F) observed

at 3000×, 6000×, and 12,000× magnification, respectively. Scale bars represent 20 (A,B); 10 (C,D), and 5 µm (E,F).

5.4 Discussion

<u>Study of CPS, EPS, string formation, rmpA</u>

Numerous individual reports are available on CPS, string test and *rmpA* in *Klebsiella* isolates from liver abscess conditions (Whitfield et al., 2020; Tai et al., 2020; Hsu et al., 2011; Yu et al., 2006;). However, no study has collectively presented the correlation between CPS and EPS production, and influence of *rmpA*, EPS, CPS in resistance of phagocytosis to determine the virulence in *Klebsiella* isolates from UTIs. The literature of string phenotype and its role in virulence is also ambiguous. On one hand there are reports claiming that string positive phenotype plays role in hypermucoviscosity, hypervirulence and resistance to phagocytosis in case of liver abscess conditions (Lin et al., 2011; Fang et al., 2004). On other hand, a recent study had reported that string phenotype may not be responsible for hypervirulence, but siderophores such as aerobactin and yersiniabactin plays role in virulence of the isolates (Catalán-Nájera et al., 2017). *rmpA* expression is reported to be crucial factor for serum resistance (Cheng et al., 2010; Fang et al., 2004., Ku et al., 2008; Yu et al., 2006 and 2008) whereas others have reported that serotypes are important determinants in resistance to phagocytosis than *rmpA* (Wang et al., 2021; Yeh et al., 2007; Lin et al., 2004). Further, the existing reports mainly focused on liver abscess conditions and other septic metastatic complications and the scenario in case of UTI is still underreported. Here, we extracted and estimated CPS and EPS, studied *rmpA* and also determined serotype of clinical isolates from UTIs; we selected isolates with important phenotypes to study effect of different virulence factors such as CPS, EPS, *rmpA* and string phenotype on phagocytosis.

We found that all uro-pathogenic isolates did not produce high amount of CPS as in our study, clinical isolates of UTIs produced a wide range of CPS (5.2 µg CPS/mg protein to 116.38 µg CPS/mg protein). Amount of EPS produced by

the isolates was almost similar (figure 5.4). In *Klebsiella*, capsule production is encoded by 26kb long *cps* gene cluster and synthesized by *wzy* dependent polymerization pathway (Pan et al., 2013). EPS are synthesized by three main pathways, namely, the ATP-binding cassette (ABC), the synthase-dependent pathway and *wzy* dependent polymerization pathway (Whitfield et al., 2020). Hence, *wzy* dependent polymerization pathway is the common pathway by which both CPS and EPS are synthesized. Therefore, we investigated if production of CPS and EPS are correlated. We found no correlation between CPS and EPS production in uro-pathogenic isolates of *Kp*, suggesting that though CPS and EPS synthesize by a common pathway their production is differentially regulated. Biofilm formation, quantity of CPS and survival in macrophages are reported to be decreased in tigecycline-resistant mutants (Park et al., 2020). While we did not observe the same phenomenon our two tigecycline-resistant isolates (DJ and M17B); the CPS quantity of DJ was 76.44 µg CPS/mg protein (relatively high; median 23.052) and M17B 16.17 µg CPS/mg protein (relatively low; median 23.052); biofilm formation by DJ and M17B was moderate and weak respectively. Other factors are also reported to be associated with CPS production and biosynthesis, for an instance, transcription regulator KP1_RS12260 (KbvR) is reported to be involved in CPS production as deletion of KbvR resulted in decreased CPS production. It has been also shown to contribute to virulence by defending against phagocytosis by macrophages (Xu et al., 2021).

Further, Fumarate nitrate reduction regulator is known to regulate CPS synthesis in anaerobic conditions (Lin et al., 2019). Lin et al., observed that CPS amount in *K. pneumoniae* increased in anaerobic conditions, compared to that in aerobic conditions. Further, they also reported that RmpA and RmpA2 participated in the holo-FNR (Fumarate nitrate reduction regulator with 4Fe-4S cluster) -mediated repression of CPS biosynthesis, and resistance to the host defence in response to oxygen availability (Lin et al., 2019).
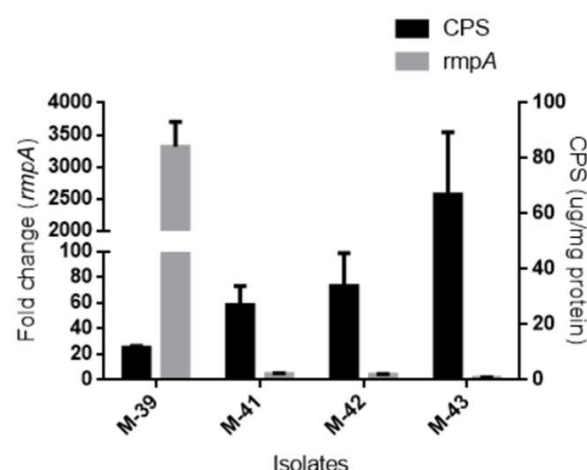
Figure 5.17 Association between CPS and *rmpA* expression. Left X-axis shows foldchange of *rmpA* overexpression (grey bars), right y-axis shows amount of CPS (black bars) produced by *rmpA* carrying isolates (x-axis).

Hypermucoviscosity is determined by string formation (Lin et al., 2011) and high production of CPS is responsible for string positive phenotype of an isolate (Cheng et al., 2010; Yu et al., 2006). However, in our study, we observed that the string positive isolate (M20) produced very low amount of CPS. Also, isolates with highest CPS production (M34) was string negative. Choi and Ko, demonstrated that colistin-resistant mutants with deletion of Δ*phoQ* and Δ*pmrB* led to decreased CPS production and string negative phenotype. They also reported that colistin resistance was accompanied by reduced CPS production, string negative phenotype and impaired virulence (Choi and Ko, 2015). However, we observed that our colistin-resistant isolate, DJ produced higher amount of CPS than average CPS production by other isolates (figure 5.1). Δ*kvrA* and Δ*kvrB* as well as Δ*rmpA* and Δ*rcsB* deletion mutants were found to affect the string test as the string test became negative in the mutants. However, Δ*rmpC* showed no change in string phenotype (Walker et al., 2019). However, the precise factors regulating the string phenotype is still unknown.

Further, it is also reported that apart from CPS, increased expression of *rmpA* determines string positive phenotype (Cheng et al., 2010). We, not only observed absence of string formation in the isolates with overexpression of *rmpA* (M39, M41, M42, M43) but also that string positive isolate (M20) did not carry *rmpA*. Hence, we report that the amount (high or low) of CPS or

presence/expression of *rmpA* do not determine string positive phenotype of an isolate. Our results are in corroboration with Yang et al., who also negate the possibility of involvement of *rmpA* in hypermucoviscosity and string formation (Yang et al., 2019). However other factors such as the variations in the composition of lipopolysaccharides (LPS) or environment inside host might influence the development of a hypermucoviscous phenotype (string formation) of bacterial isolate as reported previously (Köck et al., 2018; Shon et al., 2013

High prevalence of *rmpA* in *Klebsiella* isolates from liver abscess and low prevalence in isolates from bacteraemia is reported (Tan et al., 2019; Qu et al., 2015; Hsu et al., 2011; Yeh et al., 2007). Here, in case of clinical isolates from UTIs, we found low prevalence of *rmpA*. Numerous reports suggested that *rmpA* is a key factor responsible for hypervirulence as it leads to elevated CPS production (Zhang et al., 2019; Lin et al., 2008; Nassif et al., 1989); N-terminal region of *rmpA* was reported to interact with RcsB for CPS regulation (Cheng et al, 2010). Strong correlation between the presence of *rmpA* and hypervirulence has made *rmpA* a key biomarker for hvKp (Russo et al., 2018; Yu et al., 2018). Previous studies have also shown that loss of *rmpA* decreases *cps* gene expression and reduces hypervirulence of hvKp (Cheng et al., 2010; Hsu et al., 2011). Hence, we studied presence and expression of *rmpA*. In our study, in *rmpA* positive isolates, the expression of *rmpA* was found to be negatively associated with production of CPS as isolate with extreme overexpression of *rmpA* produced low amount of CPS (M39; 3315 folds) compared to CPS produced by the isolates with less overexpression of *rmpA* (M41, 42 and M43; ~4 folds) (figure 5.17). This was observed in *rmpA* positive isolates only, but *rmpA* negative isolates also produced extremely high (M34) and low (M10) CPS. These findings suggest that the CPS is differentially regulated in presence and absence of *rmpA*. Recent report suggested that RmpA-associated phenotypes are largely due to RmpA activating the expression of *rmpD* (*rmpD* gene is located between *rmpA* and *rmpC*) to produce hypervirulence and *rmpC* to stimulate *cps* expression (Walker et al., 2020). Further, they reported that RmpD is a small protein essential for hypervirulence (Walker et al., 2020). Walker et al., also reported that RmpC mutants lead to reduced expression of CPS but the strain still remains hypervirulent; this

suggests that capsule and hypervirulence could be two separate traits (Walker et al., 2019). Role of Fumarate nitrate reduction regulator (FNR) is also discovered in regulation of CPS synthesis via RmpA and RmpA2. The report suggested that RmpA and RmpA2 take part in the holo-FNR ([4Fe–4S] cluster of FNR)–mediated repression of CPS biosynthesis, and resistance to the host defence in response to oxygen availability (Lin et al., 2019). According to Zhang et al., *aerobactin*, *rmpA*, *mrkD*, *fimH*, *uge*, *ureA*, *entB*, *ybtA*, *kfuBC*, and *wcaG* are important virulence genes. Moreover, they reported that hypervirulence phenotype of hvKp is because of *rmpA* and aerobactin; K1/K2 serotypes are not always associated with hypervirulence (Zhang et al., 2019). Expression of *rmpA* could affect exopolysaccharide production as rmpA was reported to be a transcriptional activator of the wzy_{KpK1} *cps* loci (Chuang et al., 2006), and wzy KpK1 (previously known as magA) is responsible for exopolysaccharide web biosynthesis gene (Yeh et al., 2010). However, in this study, isolates with overexpression of rmpA did not show very high amount of *rmpA* (M39, M41, M42) and isolates with highest amount of EPS did not even carry *rmpA* (M27, ST-1) (figure 5.2).

Phagocytosis is one of the major mechanism of *Klebsiella* pathogenesis to invade host immune system and a valid indicator of bacterial virulence and CPS is reported to play role in inhibition of phagocytosis (Clegg et al., 2016; Lin et al., 2004). Initial studies reported that mucoid phenotype (M-type) is a virulence factor and resist phagocytosis (Victor et al., 2007; Nassif et al., 1989). But we observed that majority of our isolates were having mucoid appearance, but they were not able to resist the phagocytosis; therefore, mucoidity does not play role as an independent virulence factor. *rmpA* expression is reported to be crucial factor for serum resistance (Cheng et al., 2010; Fang et al., 2004., Ku et al., 2008; Yu et al., 2006 and 2008), whereas Yeh et al, reported that K1 K2 are major virulence determinants than *rmpA* and *magA* (Yeh et al., 2007). However, we did not observe high resistance to phagocytosis in isolate with highest expression of *rmpA* (M39) compared to other isolates (figure 5.9). Further**,** we performed phagocytosis assay to evaluate the role of amount of CPS and EPS in resistance of phagocytosis as role of high amount of CPS and EPS had been described previously (Cheng et al., 2010; Fang et al., 2004). We report

that amount of CPS or EPS produced by the isolates (high or low) does not affect the amount of phagocytosis. Our results support hypothesis by Lin et al., who also reported that the amount of CPS does not affect resistance to phagocytosis of an isolate, but the serotype does (Lin et al., 2006). Further, Hsu et al., also reported that although capsule is important for pathogenesis, at least in the hypervirulent *Kp* (hvKp) strain NTUH-K2044 with K1 serotype, increased capsule production did not affect virulence (Hsu et al., 2011). However, the type of CPS, mainly K1 and K2 are reported to be capable of inhibiting phagocytosis more than non K1/K2 isolates. (Lin et al., 2004; Fung et al., 2002). Recently, Wang et al., demonstrated that isolates belong to K1 and K2 as well as ST11 despite of sharing similar virulence gene profiles, ST11 isolates showed less serum and phagocytic resistance than the serotype K1/K2 isolates (Wang et al., 2021). In contradiction to this, we observed that inhibition of phagocytosis was less in K2 isolate (M27) than non-K2 isolates, M20 (K39) and M10 (K23). Regarding the role of K1-K2 and hypervirulence of *Kp*, K1 or/and K2, were initially proposed to be defining characteristics of hvKp (Fang et al., 2007; Fung et al., 2002; Yeh et al., 2007). However, recent studies have demonstrated that a number of hvKp strains possess non-K1, K2 capsular serotypes (Brisse et al., 2009; Yu et al., 2011). Further, regarding hypervirulence, M20 being a string positive isolate, could be considered as a hypervirulent isolate based on previous definitions of hvKp (Fang et al., 2004). However, Choby et al., reported that isolates with increased capsule production, K1 and K2 capsule types, and the colibactin toxin is considered to be hvKp (Choby et al., 2020); Also, capsular mutants showed more significant decrease in lethality than aerobactin mutants in case of hvKp (Wang et al., 2021). Other studies reported that isolate with *rmpA* and/or aerobactin and are considered as hypervirulent (Lan et al., 2021; Zhang et al., 2019; Paczosa and Mecsas, 2016; Liu and Guo, 2019; Catalán-Nájera et al., 2017). Catalán-Nájera et al., also explained that hypervirulence and hypermucoviscosity are two different phenotypes, all hypervirulent isolates are not necessarily hypermucoviscous and vice-versa (Catalán-Nájera et al., 2017); hence, according to the recent reports M20 could be considered as hypermucoviscous but not as hvKp. Although, interestingly, we observed the least phagocytosis in the isolate with string positive phenotype (M20) than the isolates with highest overexpression of *rmpA*

(M39, 3315-fold overexpression) as well as high amount of CPS with negative string phenotype (M34, M43) (figure 5.9). Therefore, string positive phenotype of the isolate might play a role in inhibition of phagocytosis as reported previously (Cubero et al., 2016; Fang et al., 2004). Hence, all string positive phenotype might not be solely responsible for higher resistance to phagocytosis as there are other factors involved such as adhesins present on bacterial cell surface (Hart., 2006; Pruzzo et al., 1989). However, isolates with string positive phenotype do provide warning signal that the strain could be more virulent. Limitation of the study is that we could get only one isolate with string positive phenotype; in UTI isolates string positive phenotype is not encountered very commonly as in liver abscess condition (Zhang et al., 2019; Tan et al., 2019; Luo et al., 2014; Hadano., 2013; Vila et al., 2011). Importantly, Wang et al., demonstrated that, to avoid confusions, strains should be considered as hvKp based on animal studies only as significant difference was observed in in-vitro and *in vivo* models. Here, we have demonstrated virulence of the isolates with different phenotypes *in vitro* only. Hence, to determine role of string phenotype in virulence, further animal studies are warranted (Wang et al., 2021). Further, we have focused on virulence factors such as CPS, EPS, expression of *rmpA* and string phenotype and other virulence factors like siderophores have not been included in this study.

Study of Biofilm

Regarding the study of biofilms, despite biofilm formation by *Kp* has been extensively studied (Karimi et al., 2021; Diago-Navarro et al., 2014; Nicolau et al., 2013; Revdiwala et al., 2012; Anderl et al., 2003; Zahller et al., 2002) the mechanism of strong biofilm formation in *Kp* is underexplored. Moreover, how strong and weak *Kp* biofilm differ from each other is unclear. The present study extends the knowledge about constituents contributing to strong *Kp* biofilms. In this study, clinical isolates from UTIs showed varying levels of biofilm formation in the CV assay. Furthermore, the biofilm index (Biofilm index = OD570(CV assay)/OD 600(culture)) and OD of bacterial culture after 24 h of biofilm formation, before washing of unbound cells was measured to validate that the difference in biofilm formation is not because of difference in the growth rate of the bacteria (Crémet et al., 2013). Further, no difference in

growth rate was found in strong and weak biofilm producers (figure 5.11B). Variation in the rate of biofilm formation, stages of biofilm formation, and structural differences between strong and weak biofilm have been reported previously (Balestrino et al., 2008).

Results of biofilm formation on latex, silicone-coated latex and silicone catheters show high, moderate, and low biofilm formation, respectively. Another important observation was that *Kp* isolates with weak biofilm forming capacity formed a strong biofilm on latex urinary catheters. The issue with latex is its cytotoxicity in addition to increased biofilm formation. Hence, latex catheters are now coated with silicone elastomer to reduce this risk. Many modern catheters are made entirely of silicone and hydrophilic coatings, which are used to provide a slippery surface to reduce attachment (Feneley et al., 2015). Lee et al., have reported that the rough surface of latex catheters makes the microbial attachment easy and an additional amount of biofilm formation occurs, whereas smooth surface and less hydrophobicity of silicone catheters are responsible for reduced biofilm formation (Lee et al., 2017). Our results corroborate with these findings in favor of silicone catheters to be preferred over latex with respect to biofilm formation. However, the cost of latex catheter is five times lower than silicone catheters and hence, latex is coated with silicone and is the preferred choice in clinical settings of most developing countries. To increase the resemblance with the clinical scenario in developing countries, quantification of biofilm on silicone-coated latex catheters (widely used catheters) in the presence of urine was performed. Composition of growth medium and substratum are known to have influence on the production of extracellular components and biofilm density (Bandeira et al., 2017) and our findings further validate these reports.

The second aim of the study was to quantify and compare the components of weak and strong biofilms. Results in the present study show high eDNA, protein, EPS, cell adhesion, and unusual cell death in strong biofilms. Detailed studies on *Pseudomonas aeruginosa* biofilms have shown that eDNA forms complexes with exopolysaccharides (Hu et al., 2012) and crosslinks with proteins (Huseby et al., 2010; Domenech et al., 2013). This increases mechanical strength and adhesion capacity of the bacteria by acid-base

interaction with the surfaces (Okshevsky et al., 2015). Moreover, polysaccharides, proteins, and DNA allow the initial steps in the colonization and temporary immobilization of bacterial cells to the surfaces (Flemming and Wingende, 2010; Jakubovics et al., 2013). Presence and importance of eDNA in *Kp* biofilms was shown by giving DNase treatment which led to reduced biofilm formation (Tetz et al., 2009). Harmsen et al., have also done the experiments with the addition of salmon sperm DNA, genomic DNA, and DNase I in biofilm formation of *Listeria monocytogenes*. Significantly reduced biofilm was observed upon the treatment with DNase I. However, no significant increase was reported in case of addition of genomic DNA or salmon sperm DNA. They also concluded that the size of the intercellular molecules matters and reducing the size of these molecules and addition of the single components do not increase adhesion or biofilm formation (Harmsen et al., 2010). Our results with *Kp* biofilms corroborate with these reports, that in *Kp* biofilms, significant reduction was observed upon treatment with DNase I, as well as no significant increase was seen upon the addition of *Kp* genomic DNA. In addition to DNase I, no significant effect in the presence of RNase A and Proteinase K was reported in case of *Listeria monocytogenes* (Harmsen et al., 2010). However, we have observed significant reduction in both weak and strong biofilms upon treatment with Proteinase K. Moreover, biofilm was significantly reduced after treatment of RNaseA in case of strong biofilms.

Preliminary observations of increased cell death in strong biofilms came from the results of the resazurin assay. Further, flow cytometry and CLSM were performed to confirm these observations. The difference between % cell death measured by flow cytometry and CLSM is due to difference in the experimental procedure of live dead assay. Cell death has been reported to be crucial in case of *S. aureus* and *P. aeruginosa* biofilms (Bayles et al., 2007). The multicellular structure of biofilm provides a selective pressure for programmed cell death which eliminates damaged cells and enhances nutrient availability for the healthy cells in the biofilm matrix (Lewis., 2009). Cell death is caused by self-destruction of individual cells and lysis of dead bacteria releases genomic DNA (Claverys and Håvarstein, 2007). Except programmed cell death, several other mechanisms are reported for eDNA release such as membrane vesicle formation

(Renelli et al., 2004), prophage-mediated cell death in *Pseudomonas aeruginosa* (Webb et al., 2003), and specialized secretion in *Neisseria gonorrhoeae* (Salgado-Pabón et al., 2010). However, in *Kp* the mechanism for the release of eDNA is unclear. We hypothesize that cell death could be the cause of increased eDNA, protein, and EPS in strong biofilms. The arrangement observed in the 3D structure of confocal microscopy indicates that dead cells could act as physical barriers protecting the live cells inside the matrix. Cell death during biofilm formation is an ordered and well-regulated process (Bayles et al., 2007). Though cell death during biofilm formation is one of the least understood processes; three models have been proposed that lead to cell death (Fagerlind et al., 2012). 1. Bacteria at the base of the microcolony die as nutrients are unable to reach the innermost layer of the biofilm. 2. Bacteria even in the outer layers of the biofilm die and metabolism of the neighboring bacteria seem to contribute to death. 3. Bacteria die due to accumulation of damage at the top of the microcolony. Any of the above-mentioned theories could be playing a role simultaneously during *Kp* biofilm formation. Thus, what causes such increased cell death warrants further investigation.

In addition to all these factors, fimbriae is also reported as one of the factors associated with biofilm formation. Previously it is also reported that both, type 1 and type 3 fimbria-encoding operon is found in and expressed by almost all *Kp* isolates in biofilm state and both, type 1 and type 3 fimbriae play a role in the formation of biofilm (Stahlhut et al., 2012; Paczosa and Mecsas, 2016). In our study, *fim* gene cluster encoding type 1 fimbriae and *mrk* gene cluster (*mrkABCD*) encoding type-3 fimbriae were found to be present in whole genome of all six isolates (both strong and weak biofilm producers) (data not shown). Hence, absence of fimbriae can prevent biofilm formation, but it may not be solely responsible for either strong or weak biofilm. Recently, SdiA, a quorum-sensing regulator has been reported to regulate cell division and suppress the expression of fimbriae expression as well as biofilm formation (Pacheco et al., 2021).

Regarding antibiotic resistance and biofilm forming capability, Fang et al., reported that *mrkH* has plays a crucial role in biofilm formation and suggested that carbapenem-resistant *Kp* is less likely to have strong biofilm-forming

capacity because it does not carry the *mrkH* gene (Fang et al., 2021). In contradiction to this report, all four of our carbapenem-resistant isolates (M2, M6, M17B and DJ) were found to carry *mrkH* (based on Illumina NGS sequencing), and they were also moderate or strong biofilm producers. Hence, carbapenem-resistance does not seem to be associated with *mrkH* distribution and low capacity of strong biofilm formation. Further, we have no evidence to indicate that disease severity correlates with strong or weak biofilm formers, we do not claim the "strong" to be associated with disease severity or its ability to withstand the biophysical stress.

Bandeira et al., had studied the ability of various *Kp* strains to assemble biofilms and relative area occupied by bacteria and extracellular polymeric substances on cell culture plates using SEM. They have categorized the strains into most and the least efficient, as well as intermediately efficient biofilm assembler (Bandeira et al., 2014). Singla et al., have shown 3D structure of *Kp* biofilms with enhanced exopolysaccharide production and water channel formation (Singla et al., 2014). Here, we report SEM of weak and strong *Kp* biofilms grown on silicone-coated latex catheters with more number of bacteria and increased EPS in strong biofilm compared to weak.

To summarize, Clinical isolates of *Kp* from UTIs produce a wide range of CPS and EPS. All pathogenic isolates do not produce higher CPS and/or EPS. String positive phenotype is not associated to *rmpA* or higher amount of CPS production. Amount of CPS, EPS or overexpression of *rmpA* do not affect the ability of an isolate to resist phagocytosis. Further, isolates with non-K2 serotypes showed more resistance to phagocytosis than K2. hypermucoviscous isolate with string positive phenotype (M20) was observed to affect the ability of resistance to phagocytosis and string phenotype may play a role in virulence. In case of biofilms, we found that clinical isolates of UTIs form heterogenous biofilms. Biofilm formation is increased on latex catheters and reduced biofilm formation was observed on silicone catheters or silicone-coated latex catheters. High eDNA, protein, EPS, cell adhesion, and unusual cell death were found to be associated with the strong biofilms.